Late-Paleozoic emplacement and Meso-Cenozoic reactivation of the southern Kazakhstan granitoid basement

Elien de Pelsmaeker, Stijn Glorie, Mikhail M. Buslov, Fedor I. Zhimulev, Marc Poujol, Valery Korobkin, Frank Vanhaecke, Evgeny V. Vetrov, Johan de Grave

Late-Paleozoic emplacement and Meso-Cenozoic reactivation of the southern Kazakhstan granitoid basement

Elien De Pelsmaeker[1,*], Stijn Glorie[2], Mikhail M. Buslov[3, 4], Fedor I. Zhimulev[3], Marc Poujol[5], Valeriy V. Korobkin[6], Frank Vanhaecke[7], Evgeny V. Vetrov[3], Johan De Grave[1]

[1] Department of Geology and Soil Science, Ghent University, Ghent, Belgium

[2] Tectonics, Resources and Exploration (TraX), Department of Earth Sciences, University of Adelaide, Adelaide, Australia

[3] Institute of Geology & Mineralogy, Siberian Branch, Russian Academy of Sciences, Novosibirsk, Russia

[4] Novosibirsk State University, Novosibirsk, Russia

[5] Université de Rennes 1, Laboratoire Géosciences Rennes, UMR 6118 CNRS, Rennes, France

[6] Department of Geology and Physics of the Earth, Kazakh-British Technical University, Almaty, Kazakhstan

[7] Department of Analytical Chemistry, Ghent University, Ghent, Belgium

* Corresponding author:

Department of Geology and Soil Science, Ghent University

Krijgslaan 281.S8, WE13, B-9000 Gent, Belgium

Elien.DePelsmaeker@UGent.be

Abstract

The Ili-Balkhash Basin in southeastern Kazakhstan is located at the junction of the actively deforming mountain ranges of western Junggar and the Tien Shan, and is therefore part of the southwestern Central Asian Orogenic Belt. The basement of the Ili-Balkhash area consists of an assemblage of mainly Precambrian microcontinental fragments, magmatic arcs and accretionary complexes. Eight magmatic basement samples (granitoids and tuffs) from the Ili-Balkhash area were dated with zircon U-Pb LA-ICP-MS and yield Carboniferous to late Permian (~350-260 Ma) crystallization ages. These ages are interpreted as reflecting the transition from subduction to (post-) collisional magmatism, related to the closure of the Junggar-Balkhash Ocean during the Carboniferous – early Permian and hence, to the final late Paleozoic accretion history of the ancestral Central Asian Orogenic Belt. Apatite fission track (AFT) dating of 14 basement samples (gneiss, granitoids and volcanic tuffs) mainly provides Cretaceous cooling ages. Thermal history modeling based on the AFT data reveals that several intracontinental tectonic reactivation episodes affected the studied basement during the late Mesozoic and Cenozoic. Late Mesozoic reactivation and associated basement exhumation is interpreted as distant effects of the Cimmerian collisions at the southern Eurasian margin and possibly of the Mongol-Okhotsk Orogeny in SE Siberia during the Jurassic – Cretaceous. Following tectonic stability during the Palaeogene, inherited basement structures were reactivated during the Neogene (constrained by Miocene AFT ages of ~17–10 Ma). This late Cenozoic reactivation is interpreted as the far-field response of the India-Eurasia collision and reflects the onset of modern mountain building and denudation in southeast Kazakhstan, which seems to be at least partially controlled by the inherited basement architecture.

Keywords (max. 6): Ili-Balkhash; Zircon U-Pb dating; Apatite fission track thermochronology; Junggar; Tien Shan; Dzhungar

1. Introduction

The Ili-Balkhash Basin (IBB) is a Meso - Cenozoic foreland basin to the growing Tien Shan and West Junggar orogens, situated in SE Kazakhstan (Fig. 1). It is separated from the Chinese Junggar Basin (E) by the Kazakh - Chinese West Junggar Mountains and continues southeast in the Chinese Ili Basin (Fig. 1). To the west, the basin is bounded by the vast Kazakhstan paleocontinent and to the northeast, at the border zone with Siberia, by the Altai - Sayan Mountains (Fig. 1). The Trans-Ili and Kungey mountain ranges are part of the Kazakh - Kyrgyz Tien Shan and separate the IBB from the intramontane Issyk-Kul Basin to the south (Fig. 2).

The IBB is located in the southwestern part of the Central Asian Orogenic Belt (CAOB) (Fig. 1). The CAOB represents one of the largest Phanerozoic accretionary orogens in the world and stretches from North China - Tarim, through Kazakhstan to the Siberian craton (Korobkin and Buslov, 2011; Şengör et al., 1993; Windley et al., 2007). The CAOB can be regarded as a complex collage of different terranes: mainly fragments of microcontinents, arc and accretionary complexes. These were amalgamated during several Paleozoic accretion-collision events, and associated magmatic episodes, in relation to the closure of the Paleo-Asian Ocean (e.g. Alexeiev et al., 2011; Buslov, 2011; Dobretsov and Buslov, 2007; Filippova et al., 2001; Korobkin and Buslov, 2011; Wilhem et al., 2012; Windley et al., 2007, Xiao et al., 2013). Final amalgamation of the CAOB took place in the Permian and was accompanied by significant (post-) collisional tectonic and magmatic activity (e.g. Wang et al., 2009a; Wilhem et al., 2012). During the Mesozoic and Cenozoic, parts of the CAOB were periodically reactivated in response to distal tectonic events, with a final (and still active) late Cenozoic shortening phase related to the India-Eurasia collision (e.g. De Grave et al., 2007; Dumitru et al., 2001; Jolivet et al., 2010). Hence, as a consequence of the large-scale reactivation of the CAOB, the present-day topography is dominated by intracontinental mountain ranges (mainly consisting of deformed Precambrian and Paleozoic basement) separated by intramontane and foreland basins which are mainly characterized by Meso - Cenozoic sedimentary deposits.

Although absolute radiometric age information on the surrounding (mainly basement) area, i.e. the Kyrgyz Tien Shan (e.g. Bullen et al., 2001; De Grave et al., 2011a, 2012, 2013; Glorie et al., 2010, 2011b; Konopelko et al., 2007; Macaulay et al., 2014), the Chinese Junggar (e.g. Hendrix et al., 1992; Shen et al., 2012; Zhou et al., 2008) and the southern Altai (e.g. Glorie et al., 2011a, 2012a, 2012b; Tong et al., 2014) has augmented our knowledge of the broader region, still little is known about the geodynamic evolution of the IBB, and absolute age data from the border zone of the aforementioned terranes is lacking. In this perspective, we present twenty-two new ages (8 zircon U-Pb and 14 apatite fission-track ages) from basement samples collected around the IBB in SE Kazakhstan. Sampled basement ranges include the adjacent Kazakh West Junggar (or Dz(h)ungarian), Trans-Ili (or Zailisky), Zhetyzol and Chu-Ili mountains (Fig. 2). The results will be placed in a broader geodynamic framework based on available data in order to gain a better understanding of the thermo-tectonic history of the southeastern Kazakh basement with the future aim of constraining provenance indicators for Meso - Cenozoic sediment sources in the IBB.

2. Geological setting

The IBB is located at the southeastern edge of Kazakhstan, at the junction of the Kazakh - Chinese West Junggar Mountains and the Kyrgyz - Chinese Tien Shan, which are part of the southwestern CAOB (Fig. 1 and 2). The West Junggar Mountains form the southwestern boundary of the triangular-shaped Junggar Basin and are largely composed of Paleozoic magmatic arcs and accretionary complexes that amalgamated during the late Paleozoic (Korobkin and Buslov, 2011; Shen et al., 2012; Xiao et al., 2008). Our study area partly encompasses the Kazakh West Junggar Mountains, which can be viewed as the westward topographic continuation of the Chinese West Junggar Mountains, more or less west of the Junggar Fault (Fig 2).

The currently reactivated intracontinental Tien Shan orogen extends from West to East through Uzbekistan, Kazakhstan, Tajikistan, Kyrgyzstan and China (Xinjiang province) over a distance of more

than 2000 km (Fig. 1). The Tien Shan is subdivided in different tectonic units, but cross-boundary correlation and nomenclature through the aforementioned countries is often not uniform. Traditionally, the western Tien Shan (post-Soviet states) is divided into three tectonic units: the North Tien Shan (NTS), Middle Tien Shan (MTS) and South Tien Shan (STS) units (e.g. Biske et al., 2013; De Grave et al., 2012, 2013; Glorie et al., 2010, 2011b; Seltmann et al., 2011) (Fig. 2). The NTS mainly consists of Precambrian microcontinental fragments, intruded by early Paleozoic granitoids (Korobkin and Buslov, 2011; Glorie et al., 2010) (Fig. 3). The MTS basement is mainly composed of Precambrian crust, covered with early - middle Paleozoic sediments and intercalations of late Paleozoic granitoids (De Grave et al., 2013; Konopelko et al., 2007; Seltmann et al., 2011). The STS represents a late Paleozoic accretionary complex, related to the collision of paleo-Kazakhstan with Tarim during the late Paleozoic (Glorie et al., 2011b; Konopelko et al., 2007; Seltmann et al., 2011). Our study area is situated along the northern edge of the Kyrgyz NTS terrane, which can be continued eastwards to the Chinese North and Central Tien Shan assemblage (Fig. 2). The latter can be considered as an amalgamated unit existing of Precambrian continental fragments, Paleozoic island arcs and accretionary complexes (Biske et al., 2013; Han et al., 2011; Xiao et al., 2013). The detailed correlation between the Kyrgyz and Chinese Tien Shan units is still a matter of debate (e.g. Biske et al., 2013; Xiao et al., 2010, 2013) and falls beyond the scope of this paper.

2.1 Paleozoic amalgamation of the Kazakhstan paleocontinent

During the early Paleozoic, the paleo-Kazakhstan basement assemblage was formed by successive amalgamations of Precambrian microcontinents (likely of an Eastern Gondwana origin), and Cambrian to early Silurian island arcs (Dobretsov and Buslov, 2007; Windley et al., 2007). These numerous early Paleozoic accretion-collision events and associated magmatic episodes gave rise to the formation of the Kazakhstan paleocontinent by the late Silurian (Alexeiev et al., 2011; Bazhenov et al., 2012; Biske et al., 2013; Filippova et al., 2001; Korobkin and Buslov, 2011; Wilhem et al., 2012; Windley et al., 2007; Xiao et al., 2010; Zhao and He, 2013). As a result, early Paleozoic granitoids

associated with the collision-accretion events constructing the Kazakhstan paleocontinent, can be found across the Kazakhstan and NTS basement (e.g. De Grave et al., 2013; Degtyarev, 2011; Degtyarev et al., 2006; Glorie et al., 2010; Korobkin and Buslov, 2011) (Fig. 3).

Following its amalgamation, the Kazakhstan paleocontinent remained emerged during most of the Silurian and early Devonian, and drifted northwards until the Permian (Wilhem et al., 2012; Windley et al., 2007). During the middle and late Paleozoic, the paleocontinent was isolated from Siberia, Europa and Tarim, and surrounded by the Ob-Zaisan (NW), Uralia (SW), Turkestan (SE) and Junggar-Balkhash (NE) oceans (e.g. Filippova et al., 2001; Korobkin and Buslov, 2011; Windley et al., 2007) (Fig. 3b). These oceans are considered as sub-basins of the Paleo-Asian Ocean. The ensuing tectonic history of the Kazakh paleocontinent is then dominated by the closure of the aforementioned ocean basins and the associated Siberia – paleo-Kazakhstan – Tarim convergence. Subduction of the Junggar-Balkhash oceanic lithosphere beneath the northeastern margin of the Kazakhstan paleocontinent started in the early Devonian, resulting in a major Andean-type magmatic belt (Windley et al., 2007) (Fig. 3). By the Late Devonian, the subduction zone moved eastwards and arc magmatism continued in the Ili-Balkhash region until the late Carboniferous – earliest Permian (Filippova et al., 2001; Korobkin and Buslov, 2011; Kröner et al., 2008; Seltmann et al., 2011; Wilhem et al., 2012; Windley et al., 2007; Xiao et al., 2013). Simultaneously, to the southeast of the paleocontinent, oblique closure of the Turkestan Ocean took place from the late Carboniferous until the early Permian and resulted in the collision between Kazakhstan and Tarim (Fig. 3c). Related to the general convergent motion between Tarim and Siberia, with Kazakhstan trapped in between, Devonian - early Mesozoic oroclinal bending of the Kazakhstan paleocontinent occurred (e.g. Abrajevitch et al., 2007, 2008; Choulet et al., 2011; Levashova et al., 2007, 2012; Van der Voo et al., 2006). In addition, closure of the Ob-Zaisan and Uralian oceans led to the final collision between paleo-Kazakhstan and Siberia and Baltica respectively (Fig. 3b-c), resulting in the gradual consumption of surrounding oceanic lithosphere and final amalgamation of the ancestral CAOB by the late Permian (e.g. Buslov et al., 2004, 2013; Windley et al., 2007). More details about the

geodynamic evolution of paleo-Kazakhstan during the Paleozoic can be find in e.g. Korobkin and Buslov, 2011.

2.2 Latest Paleozoic to Cenozoic intracontinental evolution

Since the final incorporation of the Kazakhstan paleocontinent in paleo-Eurasia during the Permian, its geodynamic evolution has been dominated by intracontinental tectonics. During the late Permian – early Mesozoic, the Kazakhstan orocline became completely closed and the area was affected by (1) (post-) collisional deformation and large-scale strike-slip faulting (e.g. the Talas-Ferghana Fault, Fig. 1) related to the relative motions of Baltica, Siberia, Junggar and Tarim, and (2) tectonic far-field effects of collisions transpiring at the plate's margins several hundreds of kilometers away (Abrajevitch et al., 2008; Buslov, 2011; Buslov et al., 2003b, 2004; Choulet et al., 2011; Levashova et al., 2012; Rolland et al., 2013; Şengör and Natal'in, 1996; Van der Voo et al., 2006; Wilhem et al., 2012; Windley et al., 2007).

Also during the Permian, the type of magmatism changed from a collisional to a post-collisional setting (e.g. Biske et al., 2013; Kröner et al., 2008; Windley et al., 2007; Zhao and He, 2013). Traces of this post-collisional magmatic episode (mainly A-type and (per-)alkaline magmatism) can be found in e.g. the Kyrgyz North Tien Shan (De Grave et al., 2013; Kröner et al., 2008), the Chinese Central Tien Shan (Dong et al., 2011), the Chinese West Junggar (Shen et al., 2013a) and southern Altai (Tong et al., 2014).

During the latest Paleozoic - Mesozoic, the CAOB was repeatedly reactivated as a distant effect related to the closure of the Paleo-Tethys and/or Mongol-Okhotsk oceans (e.g. De Grave et al., 2013; Jolivet, 2015; Jolivet et al., 2010, 2013b). Evidence for these reactivation episodes is often documented in the cooling histories of the exhumed basement rocks and in the sediments of the intervening basins, but the extent of these reactivation events is still under discussion (e.g. De Grave et al., 2007; Dumitru et al., 2001; Glorie and De Grave, 2015; Jolivet et al., 2013a,b; Vandoorne et al.,

2011; Yang et al., 2015). Due to the closure of the Paleo-Tethys Ocean, several accretion-collision events took place at the southern Eurasian margin resulting in the creation of the Mesozoic Tien Shan (e.g. De Grave et al., 2013; Dumitru et al., 2001; Jolivet, 2015; Yang et al., 2013). These events are often grouped as the Cimmerian Orogeny and include collision of the Pamir–Tibetan blocks. In this context, collision of the Qiangtang block took place in the Late Triassic; the Lhasa block in the Late Jurassic - Early Cretaceous; the Karakoram block and the Kohistan-Dras arc in the Late Cretaceous. In addition, the Mongol-Okhotsk Orogenic Belt (MOOB) was formed by the diachronous oceanic closure between Mongolia – North China and Siberia during the Jurassic – Cretaceous (Metelkin et al., 2010, 2012; Wilhem et al., 2012 and references therein; Zorin, 1999). The MOOB seems to have mainly affected the areas northeast of the Tien Shan (e.g. the Altai-Sayan; Glorie and De Grave, 2015).

Following these Mesozoic reactivation episodes, the study area became tectonically more stable and evidence exists that a mature peneplain developed during the Late Cretaceous – early Paleogene (Allen et al., 2001; Bullen et al., 2001, 2003; De Grave et al., 2013; Delvaux et al., 2013; Glorie et al., 2010; Macaulay et al., 2014). Since the early Eocene, major structures in the southern CAOB were reactivated, which is likely a response to the continuous closure of the Tethys Ocean and associated accretions of island-arcs or continental slivers of `Greater India` to the southern Eurasian margin (e.g. Glorie et al. 2011b; Glorie and De Grave, 2015). From the late Oligocene – Miocene onwards, the southern CAOB was once more subjected to deformation, this time induced by the India-Eurasia collision. This is shown by low temperature thermochronology (e.g. Bullen et al., 2001; De Grave et al., 2013; Glorie et al., 2012a; Hendrix et al., 1994; Macaulay et al., 2014), sedimentology (e.g. Thomas et al., 1999), magnetostratigraphy and structural geology (e.g. Abdrakhmatov et al., 1996; Buslov et al., 2007; Campbell et al., 2013).

3. Samples and methods

3.1 Sample sites

The basement of SE Kazakhstan, and in particular the Ili-Balkhash study area, can be subdivided into different structural units based on Alexeiev et al. (2011), Kröner et al. (2013) and Windley et al. (2007) (Fig. 3a). The main units can be summarized as: (1) Kyrgyz North Tien Shan (NTS), Chu-Ili (CY) and Aktau-Junggar (AJ) Precambrian microcontinental blocks; (2) Cambrian – Ordovician Dzhalair-Naiman (DN) and Kyrgyz-Terskey (KT) accretionary complexes; (3) dispersed remnants of an Ordovician arc within the Kyrgyz NTS, KT and DN units; (4) Ordovician – Late Devonian North Balkhash (NB) accretionary complex; (5) Late Devonian – Carboniferous Junggar Balkhash (JB) accretionary complex; (6) Late Devonian – Permian Balkhash-Ili (BY) active continental margin arc and (7) Devonian to Permian epicontinental and non-marine sediments (Chu Basin). In this study, we present 22 new ages (14 apatite fission track and 8 zircon U-Pb ages) obtained on 16 basement samples (i.e. granitoids, volcanic tuff and gneiss; Table 1) collected from mountain ranges surrounding the IBB. Sampled mountain ranges are the Kazakh West Junggar, Altyn-Emel, Malaysari, Trans-Ili, Sogeti, Zhetyzol and Chu-Ili Ranges (Table 1, Fig. 2).

In the Kazakh West Junggar Mountains and neighboring ranges, Permian plutons of the Balkhash-Ili (BY) magmatic belt are exposed in the highest mountain ridges (Fig. 2, 3 and 4). These Permian granitoids cross-cut folded Devonian - Carboniferous rocks and are in their turn displaced by strike-slip faults, such as the Aktas Fault (Fig. 2 and 4). Samples 11-01, 11-07 and 11-09 were collected from these Permian granitoids, whereas samples SK-17, SK-21 and SK-22 were taken from surrounding Devonian - Carboniferous magmatic rocks (Fig. 4). Samples 11-11 (diorite) and 11-20 (granite) come from the same location in the Kazakh West Junggar Mountains, but differ in lithology and probably represent a contact zone between Permian and Devonian – Carboniferous intrusions. At the southern border of the IBB, in the Trans-Ili, Sogeti and Zhetyzol Ranges, intrusive bodies are mostly of Late Ordovician - Silurian age, while minor amounts of Carboniferous and Permian intrusive rocks are also common (De Grave et al., 2013; IGCAGS, 2006). From these mountain ranges, granitoid samples 10-20, 11-27, 11-28, SK-05A, SK-31 and SK-32 were collected (Fig. 2 and 4, Table 1). The northern

edge of the Zhetyzol Range is defined by the Dzhalair-Naiman strike-slip fault (DNF), which continues westward along the Chu-Ili Range into the Kazakhstan platform (Campbell et al., 2013) (Fig. 2 and 4). More to the south, the Trans-Ili Range is separated from the Kungey Range of the Kyrgyz Tien Shan by the Chon-Kemin-Chilik Fault system (CKCF) (Fig. 2 and 4). To the northwest of the IBB, along the northern continuation of the Chu-Ili Mountains and near Lake Balkhash, samples 10-40 and 10-42 were taken from late Paleozoic (Carboniferous – Permian) granitoid bodies (Fig. 2 and 4, Table 1).

3.2 Zircon U-Pb (ZUPb) dating

The ZUPb dating method is based on the (α, β)-decay of ^{238}U and ^{235}U to stable ^{206}Pb and ^{207}Pb, respectively. Due to its high closure temperature (>800°C, Cherniak and Watson, 2003), the ZUPb system dates the (re)crystallization of the zircon-bearing basement rock. In the case of unmetamorphosed granitoid rocks, this high-temperature method normally yields the emplacement age of the magmatic body.

For each sample analyzed, around 30-70 zircon grains were handpicked and mounted in epoxy resin, after which their surface was polished. Zircon grains were imaged for their cathodoluminescence (CL) properties, using a JEOL JSM-6400 Scanning Electron Microscope (SEM) at the Department of Geology and Soil Sciences, Ghent University, Belgium. Core-rim relationships were investigated and obvious inclusions and microfractures were avoided during further Laser Ablation – Inductively Coupled Plasma – Mass Spectrometry (LA–ICP-MS) analysis.

The ZUPb analyses were partly carried out at the LA–ICP-MS facility of the Department of Analytical Chemistry at Ghent University (samples 11-01, 11-07, 11-09), following the procedures described in Glorie et al. (2011a; 2015), and partly at the laboratory of Géosciences Rennes at the Université of Rennes 1 in France (samples 11-20, SK-05A, SK-17, SK-21, SK-22), following the procedures described below and listed in Table 2. In the laboratory of Géosciences Rennes, ablation was performed using a ESI NWR193UC laser system, powered by a Coherent ExciStar XS Excimer laser

operating at a wavelength of 193 nm. The laser repetition rate was 3 Hz and the beam diameter 25 μm. Ablated material was carried to the mass spectrometer using He gas (flow rate ~0.8l/min), and then mixed with N_2 (at ~0.04 l/min) and Ar (at ~0.85 l/min), before being introduced into the ICP source of an Agilent 7700x quadrupole-based ICP-MS instrument, equipped with a dual pumping system to enhance sensitivity. Tuning of the instrument and mass calibration were performed using NIST SRM 612 reference glass, by monitoring the ^{238}U signal and minimizing the ThO^+/Th^+ ratio (< 0.5 %). Analyses consisted of the acquisition of the ^{204}(Pb + Hg), ^{206}Pb, ^{207}Pb, ^{208}Pb, ^{232}Th and ^{238}U signal intensities. The ^{235}U abundance was calculated from the signal intensity measured for ^{238}U on the basis of a $^{238}U/^{235}U$ ratio of 137.88 (Steiger and Jäger, 1977). Each analysis consisted of a succession of ~20s background measurement prior to ablation, followed by ~60s of zircon ablation and ~10s wash out time. The analyses were performed in time-resolved mode and the raw data were corrected for Pb/U and Pb/Th laser-induced elemental fractionation and for instrumental mass discrimination by standard bracketing with repeated measurements of the zircon reference material GJ-1 (Jackson et al., 2004). Along with the unknowns, the Plešovice zircon standard (Sláma et al., 2008) was measured to monitor the accuracy. Throughout the entire measurement time, the Plešovice zircon standard provided a concordia age of 336.9 ± 2 Ma (N=17), which is in good agreement with the reported ID-TIMS age of 337.1 ± 0.4 Ma (Sláma et al., 2008). Data reduction was carried out with the GLITTER software package (Jackson et al., 2004) and in-house Excel spreadsheets to deduce the U, Th and Pb concentrations. Ages were calculated with the Isoplot software (Ludwig, 2003) and are presented in Table 3.

3.3 Apatite Fission Track (AFT) dating

Apatite fission track (AFT) dating is a low-temperature thermochronological method based on the spontaneous fission decay of ^{238}U, which is present as a trace element in the crystal lattice of apatite. By this process, the apatite lattice accumulates linear radiation damage tracks or fission tracks. At temperatures (T) lower than ~60°C, fission tracks in apatite are considered stable on geological time scales, whereas at T > ~120-140°C (e.g. Ketcham et al., 1999; Wagner and Van den

haute, 1992) the crystal lattice regenerates and the fission tracks anneal rapidly. The ~60 - 120/140°C window (± 2 - 4 km crustal depth) is known as the Apatite Partial Annealing Zone (APAZ) and depends partly on the chemical composition of the apatite crystal (e.g. Barbarand et al., 2003; Carlson et al., 1999; Green et al., 1986; Wagner and Van den haute, 1992). In this temperature window, tracks can accumulate but are progressively shortened (partial annealing), resulting in reduced mean track lengths and broader length-frequency distributions (Gleadow et al., 1986). The AFT age, based on the measurement of the spontaneous fission track density, hence records cooling of the apatite-bearing basement rock through the APAZ. In addition, the AFT length-frequency distribution is a supplementary tool to evaluate the thermal history of the rock. Hence, this allows the reconstruction of basement cooling paths (thermal history modeling; e.g. Gallagher, 2012; Ketcham, 2005; Ketcham et al., 2000), which can be linked to the exhumation history of mountain belts.

All samples were analyzed by the external detector (ED) method with thermal neutron irradiation, following the standard AFT procedure from the geochronology laboratory at Ghent University described by De Grave and Van den haute (2002), De Grave et al. (2009, 2011a) and Glorie et al. (2010). Spontaneous fission tracks in apatite were etched in a 5.5M HNO_3 solution for 20s at 21°C (Donelick et al., 1999). Irradiation was carried out in the Belgian Reactor 1 (BR1) facility of the Belgian Nuclear Research Centre in Mol. Obtained AFT ages are reported in Table 4 as conventional zeta-ages (Hurford, 1990), calculated using an overall weighted mean zeta of 229.8 ± 4.9 a.cm^2 (personal calibration factor of E. De Pelsmaeker) based on Durango and Fish Canyon Tuff apatite age standards and IRMM 540 dosimeter glasses (De Corte et al., 1998). AFT ages were also calculated as central ages and evaluated by a radial plot to check for potential multiple AFT populations (Galbraith, 1990; Vermeesch, 2009) (Table 4). Where possible, 100 horizontal confined tracks for each sample were measured on prismatic sections parallel to the crystallographic c-axis to construct length-frequency distributions, a threshold which was not always attained in this study (Table 4). For some samples, no AFT length data is available due to low spontaneous track densities and/or a low number of suitable grains. To estimate the annealing behavior of the counted grains with measured confined

track lengths, measurements of the kinetic parameter D_{par} (mean etch pit diameter parallel to the crystallographic c-axis; Carlson et al., 1999; Donelick et al., 2005) were carried out.

Thermal history modeling was performed using the HeFTy software (Ketcham, 2005), the Ketcham et al. (2007) annealing equations and the Monte Carlo search method for inverse modeling. Modeling-constraints were based on geological arguments as expected emplacement ages derived from geological maps and ZUPb and AFT ages obtained in this study. In addition, present-day ambient surface conditions were used as low temperature constraint. In the resulting models, only time-Temperature (tT) paths with "good" fits are drawn (Ketcham, 2005).

4. Results

4.1 Zircon U-Pb data

Cathodoluminescence (CL) imaging reveals oscillatory zoning for most of the analyzed zircon crystals, which is indicative for their magmatic origin (Corfu et al., 2003; Hoskin, 2000). Figure 5 presents the resulting U-Pb Tera-Wasserburg diagrams (Isoplot software; Ludwig, 2003), which are characterized by near-concordant Carboniferous - Permian zircon age clusters. Most samples in the Tera-Wasserburg diagrams show some dispersion in both $^{207}Pb/^{206}Pb$ as well as $^{238}U/^{206}Pb$ which is likely related to the presence of a small quantity of common Pb and minor zero age Pb loss respectively. As a result, their preferred formation age was calculated from the mean $^{206}Pb/^{238}U$ ratios. For each sample, weighted mean $^{206}Pb/^{238}U$ plots are shown in Figure 5 as well.

Three samples from the Altyn-Emel and Malaysari Ranges, located at the southwestern part of the Kazakh West Junggar Mountains (SK-17, SK-21, SK-22) and one from the Sogeti Range (SK-05A) yield Carboniferous zircon crystallization ages (Fig. 5 and 6, Table 3). Sample SK-05A exhibits two apparent age clusters (Fig. 5, Table 3). An older weighted mean $^{206}Pb/^{238}U$ age of 351 ± 3 Ma (MSWD = 0.15) and a younger weighted mean $^{206}Pb/^{238}U$ age of 332 ± 2 Ma (MSWD = 0.70). The older (ca. 350 Ma) age was exclusively obtained from zircon cores, while the younger (ca. 331 Ma) age comes

from zircon rims or grains without any core-rim relationships. We suggest that the age of 332 ± 2 Ma corresponds to the zircon crystallization age of sample SK-05A, while the older (ca. 350 Ma) zircons are inherited in the ~330 Ma magma.

The Tera-Wasserburg diagram for sample SK-17 displays three apparent zircon U-Pb age populations (Fig. 5). The bulk of the measurements (16 out of 25) yield a near-concordant weighted mean $^{206}Pb/^{238}U$ age of 331 ± 2 Ma (MSWD = 0.17). In addition, seven analyses yield a younger age of 311 ± 4 Ma (MSWD = 0.34) and two older zircon grains were dated as ~350 Ma. No clear core-rim relationships nor variations in Th/U ratios were observed for this sample. The excellent correlation of the older (ca. 350 Ma) zircons with the ages obtained for the zircon cores in sample SK-05A (Fig. 5), likely indicate that the ca. 350 Ma age corresponds to the age of zircon xenocrysts and that the ca. 330 Ma age corresponds to the magma crystallization age. The younger ~310 Ma analyses show more dispersion and may reflect partial Pb-loss during a later event in combination with a small quantity of common Pb in the grains. The Tera-Wasserburg diagram for sample SK-21 (Fig. 5) shows some dispersion in $^{207}Pb/^{206}Pb$ ratios, however no clear core-rim correlations were observed to identify different zircon age populations. Therefore, an overall weighted mean $^{206}Pb/^{238}U$ age of 341 ± 2 Ma (MSWD = 0.79) was calculated and interpreted as the best estimate for the crystallization age. For sample SK-22 only one clear age cluster was identified, excluding one older xenocryst of ~363 Ma (Fig. 5). Although minor dispersion in $^{207}Pb/^{206}Pb$ was observed, a statistically acceptable weighted mean $^{206}Pb/^{238}U$ age of 320 ± 2 Ma (MSWD = 0.13) was obtained which is interpreted as the crystallization age for sample SK-22.

For the central part of the Kazakh West Junggar Range, consistent early Permian zircon crystallization ages (~296-298 Ma) were obtained for samples 11-01, 11-07 and 11-20 (Fig. 5 and 6; Table 3). The Tera-Wasserburg diagram for sample 11-01 shows a rather large dispersion in both $^{206}Pb/^{238}U$ and $^{207}Pb/^{206}Pb$. Given that no clear core-rim relations were observed, a weighted mean $^{206}Pb/^{238}U$ age of 298 ± 4 Ma (MSWD = 3.1) was obtained as the preferred crystallization age. For

sample 11-07 a concordant ZUPb age of 297 ± 2 Ma was obtained. However, given the large MSWD of 9.6, a weighted mean $^{206}Pb/^{238}U$ age was calculated which is identical to the concordant age but yields a much smaller MSWD of 1.4. Sample 11-20 exhibits rather large dispersion in $^{207}Pb/^{206}Pb$ and yields a weighted mean $^{206}Pb/^{238}U$ age of 296 ± 2 Ma (MSWD = 0.85). For sample 11-09, which was taken from the same region, a younger (late Permian) ZUPb age was obtained. The Tera-Wasserburg diagram (Fig. 5) shows rather large dispersion in both $^{206}Pb/^{238}U$ and $^{207}Pb/^{206}Pb$. Therefore a weighted mean $^{206}Pb/^{238}U$ age of 260 ± 3 Ma (MSWD = 1.8) was calculated, interpreted as the crystallization age.

4.2 Apatite fission-track data

AFT ages are reported as conventional zeta- and central- ages in Table 4 and demonstrate their similarity within 1σ error (Galbraith, 1990; Hurford, 1990). In addition, all samples fulfill the chi-squared test (> 5%) and hence no indications exist for multiple apatite age populations. Therefore, only the zeta-ages will be reported in the following sections and figures. All analyzed samples from the Kazakh West Junggar, Malaysari and Altyn-Emel Ranges (11-01, 11-09, 11-11, 11-20, SK-21) exhibit Late Cretaceous (~99-77 Ma) AFT ages, except sample 11-07 which has an AFT age of 57 ± 17 Ma (Fig. 6, Table 4). For the latter sample, only six grains could be counted, leading to a less precise AFT age (Table 4). Samples 10-40 and 10-42, located NW of the IBB, yield similar Late Cretaceous (~90-74 Ma) AFT ages (Fig. 6, Table 4). From the Trans-Ili, Sogeti and Zhetyzhol Ranges, four samples (SK-05A, SK-31, SK-32, 10-20) exhibit Cretaceous AFT ages, ranging from ca. 128 to 85 Ma; whereas two samples (11-27 and 11-28) have Miocene AFT ages (~17 and 10 Ma) (Fig. 6, Table 4).

Most length-frequency distributions exhibit relatively narrow to slightly broader, more or less symmetrical to slightly negatively skewed histograms with mean track lengths (l_m) between 13.2 and 14.1 µm (standard deviations between 1.1 and 1.5 µm) (Fig. 6, Table 4). Sample 11-01 from the West Junggar Range has a lower l_m value, i.e. 11.8 µm, and is also characterized by the broadest length distribution (standard deviation of 1.8 µm; pointing to slow cooling through the APAZ) and a mean

D_{par} value of 1.6 µm (± 0.2), which is the lowest value in this study (Fig. 6, Table 4). Apatite grains with relatively low values of D_{par} (≤ 1.75 µm; Carlson et al., 1999; Donelick et al., 2005) are generally considered as fast-annealing, hence in agreement with the observed shorter track lengths. Most of the modeled samples (≥ 75%) however have apatite grains with D_{par} values > 1.75 µm, which are usually more resistant to annealing (Carlson et al., 1999; Donelick et al., 2005).

In total, eight thermal history models (THMs) were generated using the HeFTy software (Ketcham, 2005) based on samples with sufficient to acceptable numbers of horizontal confined tracks, except for sample SK-31 which has in fact an insufficient number of length data (n = 27). However, modeling is also carried out for sample SK-31 for comparison purposes seeing its similar trend. The THMs are grouped in Fig.7 by regional setting, resulting in four models for samples from the Kazakh West Junggar – Altyn-Emel Ranges (11-01, 11-09, 11-11 and SK-21) and four models for samples from the Trans-Ili – Zhetyzhol Ranges (10-20, 11-28, SK-31, SK-32). Generally, caution is needed when interpreting the THMs, because the model results are poorly constrained at temperatures outside the PAZ. For the Kazakh West Junggar – Altyn-Emel Ranges (Fig. 7a), the four THMs indicate a well-defined phase of rapid cooling during the Late Cretaceous (~100-70 Ma). This Cretaceous cooling seems to start slightly earlier (~150-120 Ma) for samples SK-21 and 11-01 based on the THMs. After this relatively rapid cooling event, a stable to very slow cooling phase during the Paleogene is observed in all four models. Finally, around the Paleogene – Neogene boundary, cooling rates seem to increase slightly, bringing the samples to ambient surface conditions.

THMs for samples SK-32 (Trans-Ili Range) and 10-20 (Zhetyzol Range) show a clear Early to middle Cretaceous cooling phase, followed by a stable period from the Late Cretaceous through the early Cenozoic (Fig. 7b). A renewed, late Cenozoic cooling event might be present in the THM of sample 10-20, starting around 20-15 Ma. The THM for sample SK-31 (Trans-Ili Range) show a main cooling phase in the Mesozoic as well, but the cooling paths are less constrained and span the whole Jurassic - Cretaceous epochs. A late Cenozoic renewed cooling is not clearly visible in the THM of the

latter sample. In contrast, in the THM of sample 11-28 (AFT age of 17 Ma) from the Trans-Ili Range as well, a pronounced late Cenozoic cooling phase is obviously present since ± 20 Ma which brought the sample to ambient surface conditions, effectively exhuming a deeper paleo-crustal level (Fig. 7b).

5. Discussion

5.1 Zircon U-Pb data

The four analyzed magmatic samples from the Altyn-Emel, Malaysari and Sogeti Ranges (SK-05A, SK-17, SK-21, SK-22) exhibit Carboniferous zircon crystallization ages between ~341-311 Ma (Fig. 5, 6 and 8). Slightly older zircon grains and zircon cores of ~350 Ma are interpreted as xenocrysts in the ~341-311 Ma magma. The other four granitoid samples (11-01, 11-07, 11-09, 11-20) from the central Kazakh West Junggar Range reveal Permian near-concordant ZUPb ages, of which three of them have consistent early Permian ages (~298-296 Ma) and one yields a late Permian age of 260 ± 3 Ma (Fig. 5, 6 and 8).

Previously obtained ZUPb ages for the Ili-Balkhash basement in SE Kazakhstan are rather limited, but Chen et al. (2012) reported three phases of pluton intrusions (335 ± 2 Ma, 308 ± 10 Ma, 297 ± 3 Ma)based on zircon SHRIMP U-Pb geochronology of skarn-related granitoids in the Sayak ore field of the Ili-Balkhash area. According to Shen et al. (2013a) two periods of ore formation in the Kazakh North Balkhash and Chinese West Junggar occurred during the late Paleozoic. A Carboniferous (328-312 Ma) porphyry Cu metallogenic event is related to calc-alkaline arc magmatism whilst early Permian (306-289 Ma) greisen W-Mo metallogenic deposits are associated with alkaline magmatism in a collisional to post-collisional context (Shen et al., 2013a). Also Chen et al. (2010, 2014) confirmed that late Paleozoic felsic magmatism occurred mainly during the late Carboniferous to earliest early Permian in that region. Generally, Carboniferous arc magmatism can be related to the subduction of the Junggar-Balkhash Ocean, which resulted in the formation of the Balkhash-Ili (BY) magmatic belt in SE Kazakhstan (Heinhorst et al., 2000; Korobkin and Buslov, 2011;

Levashova et al., 2012; Xiao et al., 2010) (Fig. 3). This subduction zone was responsible for the formation of an extensive Late Devonian - early Permian magmatic belt, of which remnants can be found in East Kazakhstan, West Junggar and the Chinese northern Tien Shan (Charvet et al., 2007; Choulet et al., 2011, 2012, 2013; Filippova et al., 2001; Kröner et al., 2008; Tang et al., 2010; Wilhem et al., 2012; Windley et al., 2007; Xiao et al., 2010, 2013; Zhao and He, 2013). In the Chinese West Junggar, most late Paleozoic plutons range in age from 360 to 280 Ma (with a peak between 340 and 300 Ma) based on zircon U-Pb ages from Gao et al. (2014), Guo et al. (2010), Han et al. (2006), Li et al. (2014), Tang et al. (2010), Wei et al. (2011) and Zhu et al. (2007). In that region, calc-alkaline arc magmatism (characterized mainly by I-type granites) dominated around ~380-305 Ma (e.g. Choulet et al., 2011, 2012, 2013; Geng et al., 2011; Shen et al., 2013b; Tang et al., 2010; Yang et al., 2014b; Yin et al., 2010, 2013; Zhou et al., 2008). The Carboniferous (~350-311 Ma) crystallization ages obtained in this study for the Kazakh West Junggar and neighboring mountain ranges, are likely related to this arc magmatism. The combined effect of oceanic closure and oroclinal bending resulted in the continuous reorientation of the magmatic belt and buckling of the active margin (Abrajevitch et al., 2008; Choulet et al., 2012, 2013; Levashova et al., 2012; Wilhem et al., 2012). Contemporaneous local extension at the periphery of the Kazakhstan Orocline resulted in the creation of small transtensional sedimentary basins, and is likely a flexural response of the oroclinal bending process (Abrajevitch et al., 2008). An example is the Chu-(Sarysu) Basin in SE Kazakhstan which accommodated more than 6 km of Devonian to Permian continental and shallow-marine sedimentary deposits (Abrajevitch et al., 2008 and references therein) (Fig. 3a).

By the early Permian, the Junggar-Balkhash Ocean was almost entirely closed (Choulet et al., 2012; Feng et al., 1989; Wilhem et al., 2012; Windley et al., 2007). During the Permian, the geodynamic setting changed to a (post-) collisional environment and the area was affected by large-scale deformation and strike-slip faulting (e.g. Abrajevitch et al., 2008; Buslov et al., 2003b; Choulet et al., 2011, 2012, 2013; Korobkin and Buslov, 2011; Levashova et al., 2012; Van der Voo et al., 2006; Wang et al., 2007). The Talas-Ferghana Fault (TFF; Rolland et al. 2013), the Irtysh Shear Zone (ISZ)

(Buslov et al., 2004; Glorie et al., 2012b) and the Chingiz-Alakol-North Tien Shan shear zone (CANTF; Choulet et al. 2011) are important examples of such strike-slip systems near our study area (Fig. 1 and 2). Deformation along the CANTF shear zone took place around 290-240 Ma, leading to a displacement of 490 km ± 250 km (Choulet et al. 2011). In the Chinese North Tien Shan, a transition from calc-alkaline arc magmatism to alkaline intraplate anorogenic (or post-collisional) magmatism occurred during the early – middle Permian (Wang et al., 2009a). In the Chinese West Junggar, transition from a Carboniferous subduction-accretion setting to a Permian post-accretion setting transpired around 305-300 Ma (Choulet et al., 2012, 2013; Gao et al., 2014; Geng et al., 2009, 2011; Tang et al., 2010; Yin et al., 2013; Zhou et al., 2008). Between ~300-250 Ma, alkaline magmatism and A-type granites dominated with minor calc-alkaline and I-type granites in an overall post-collisional setting with major strike-slip deformation and associated extensional-transtensional tectonics (Chen and Jahn, 2004; Choulet et al., 2011, 2012, 2013; Tang et al., 2010; Zhang et al., 2008; Zhou et al., 2008). Alternatively, several researchers invoke the possibility of coeval plume magmatism in the Permian (e.g. Dobretsov, 2011; Korobkin and Buslov, 2011). Novikov (2013) reports two Permian orogenic episodes for the Chinese West Junggar, based on evidences from the sedimentary record. A first episode took place around 290-275 Ma and a second phase around 265-255 Ma. These episodes are in agreement with the overall timing of collisional to post-collisional magmatism and can potentially be correlated to the early (~298-296 Ma) and late (~260 Ma) Permian ZUPb ages for the Kazakh West Junggar basement from this study. Also Kröner et al. (2008) and Shen et al. (2013a) reported the existence of Permian anorogenic, alkaline magmatism in East Kazakhstan.

In the broader Tien Shan and Altai regions, late Paleozoic granitoid intrusives are widespread as well. In the Kyrgyz Tien Shan and Chinese Central - South Tien Shan, widespread late Carboniferous - Permian collisional and post-collisional intrusions are reported by e.g. Biske et al. (2013), De Grave et al. (2013), Dumitru et al. (2001), Glorie et al. (2010, 2011a), Han et al. (2010), Konopelko et al. (2007), Liu et al. (2014), Ren et al. (2011) and Seltmann et al. (2011). In the southern Siberian Altai region, (post-) collisional intrusives are dated as late Carboniferous - early Permian

(Glorie et al., 2011a). In the Chinese Altai, Tong et al. (2014) argued that post-collisional Permian intrusives were mostly emplaced during the 287-267 Ma interval. Generally, these intrusions are related to the closure of the Turkestan and Ob-Zaisan Oceans at the southeastern and northwestern margin of the Kazakhstan paleocontinent respectively (Fig. 3b-c), leading to the late Permian final amalgamation of the ancestral CAOB (Filippova et al., 2001; Wilhem et al., 2012; Windley et al., 2007).

5.2 AFT data

The predominantly Cretaceous AFT cooling ages (Fig. 6 and 8) and THMs (Fig. 7) for the Ili-Balkhash basement samples in this study (excluding samples 11-27 and 11-28 from the Trans-Ili Range) can be explained in terms of episodic exhumation and associated basement cooling. Our results will be placed in a broader thermo-tectonic framework based on available data from studies of e.g. Bullen et al. (2001), De Grave et al. (2011a, 2013), Glorie et al. (2010), Macaulay et al. (2014) for the northern Kyrgyz Tien Shan; Dumitru et al. (2001), Jolivet et al. (2010), Hendrix (1992, 1994), Wang et al. (2009b) for the Chinese Central and Northern Tien Shan; De Grave et al. (2007, 2008, 2011b), De Grave and Van den haute (2002); Glorie et al. (2012a), Yuan et al. (2006) for the southern Altai mountains. These studies already demonstrate the existence of several reactivation periods after the final amalgamation of the ancestral CAOB in the Permian. Based on the relative consistent two-stage cooling history of our AFT dated samples (Fig. 7 and 8), the thermal history of the Ili-Balkhash basement can be generally summarized as: distinctive cooling during the late Mesozoic, followed by a slow cooling period from the latest Mesozoic through the Paleogene. A third stage of late Oligocene – early Miocene cooling might be present in some of the THMs, but is only outspoken in sample 11-28. Each of these stages will be discussed in the subsequent sections.

5.2.1 Late Mesozoic reactivation

In the Tien Shan, the oldest reported AFT ages are Triassic - Early Jurassic, but Late Jurassic and Cretaceous ages compile the bulk of the available AFT data set (De Grave et al., 2013 and

references therein; Glorie and De Grave, 2015). For the northern Kazakh Tien Shan, De Grave et al. (2013) reported Late Cretaceous and Neogene AFT ages for the Trans-Ili Range, and Late Jurassic - Early Cretaceous ages for the Zhetyzol Range. In the northern Kyrgyz Tien Shan, Early Cretaceous AFT ages are characteristic for the central Kungey Range, while many Early to Late Cretaceous AFT ages were obtained for the Terskey Range (De Grave et al., 2013; Macaulay et al., 2014; Sobel et al., 2006). Furthermore, in and around the Chinese part of the Ili Basin, Cretaceous AFT ages are reported by Jolivet et al. (2010) and north of Lake Balkhash (in the Sayak ore field) Late Cretaceous AFT ages are reported by Chen et al. (2012). Hence, the AFT age results from this study are consistent with the aforementioned previous studies, with Early Cretaceous and Miocene ages for the Trans-Ili and Sogeti Ranges, Early Cretaceous ages for the Zhetyzol Range and Late Cretaceous to early Paleocene ages for the Kazakh West Junggar Range and the region NW of Lake Balkhash (Fig. 6). Despite the consistent Cretaceous ages, it remains difficult to make well-defined regional clusters of related AFT age data. In general, the somewhat younger Late Cretaceous to early Paleocene ages (~ 99 to 57 Ma) found in and around the Kazakh West Junggar Mountains and NW of Lake Balkhash indicate that the basement there exhumed more rapidly (i.e. deeper paleo-levels are now exposed) compared to the Sogeti and Zhetyzhol Ranges more to the south, which are characterized by older Early Cretaceous AFT ages (~128 to 110 Ma).

The predominantly Cretaceous AFT ages and THMs for the Ili-Balkhash basement generally point to a late Mesozoic cooling episode associated with basement denudation. For the Kazakh-Kyrgyz northern Tien Shan, earlier published data already demonstrated the existence of Mesozoic cooling/denudation periods. A Middle Jurassic to Early Cretaceous cooling phase is identified in the Zhetyzol and Kungey Ranges, while for the Trans-Ili and Terskey Ranges a Late Cretaceous cooling phase is recognized (De Grave et al., 2013). In contrast, Macaulay et al. (2014) only identified an Early Jurassic cooling event (200-150 Ma) in the mountain ranges south of Issyk-Kul (including the Terskey Range). In the Chinese Central Tien Shan, Hendrix et al. (1992) reported three main Mesozoic cooling episodes, namely in the latest Triassic, latest Jurassic and Late Cretaceous. Dumitru et al. (2001) and

Wang et al. (2009b) also identified a late Mesozoic cooling episode for the Chinese Central Tien Shan, while Jolivet et al. (2010) reported a broad early Permian to Middle Jurassic cooling period followed by a shorter cooling pulse around the Late Cretaceous - Paleogene (65-60 Ma). This Late Cretaceous – Paleogene pulse is mostly characterized by localized uplift along major strike-slip faults south of the Chinese part of the Ili Basin (Jolivet et al., 2010). Also Li et al. (2008, 2014) reported a Cretaceous cooling event based on AFT and apatite (U-Th)/He ages of West Junggar basement rocks. Generally, these Mesozoic cooling phases in the Tien Shan are usually interpreted as far-field effects of Mesozoic collisions at the southern Eurasian margin (e.g. De Grave et al., 2007, 2013; Dumitru et al., 2001; Hendrix et al., 1992; Li et al., 2014; Wang et al., 2009b). Progressive closure of the Paleo-Tethys Ocean and subsequent collisions of the Cimmerian blocks are believed to be responsible for the various cooling and denudation episodes in southern Central Asia during the Mesozoic (collision of the Qiangtang block in the Late Triassic, the Lhasa block in the Late Jurassic – Early Cretaceous, the Karakoram block and the Kohistan-Dras arc in the Late Cretaceous; e.g. Golonka, 2004; Kapp et al., 2003; Metcalfe, 2013; Roger et al., 2010). In addition, far-field effects of the MOOB to the NE of the study area during the Jurassic – Cretaceous cannot be excluded, although its extent and influence is at present highly contested (e.g. Jolivet et al., 2010, 2013a, 2013b; Metelkin et al., 2010; Wilhem et al., 2012 and references therein). In the southern Altai Mountains, several AFT studies point to a Late Jurassic - Cretaceous basement cooling event, which is generally linked to both the Mongol-Okhotsk and the Cimmerian Orogeny during the Mesozoic (Cogné et al., 2005; De Grave et al., 2007, 2008; Glorie et al., 2012a, 2012b; Halim et al., 1998; Yuan et al., 2006). However, most authors favor the Mongol-Okhotsk Orogeny and subsequent collapse as the main driving force for the Late Jurassic – Cretaceous cooling and denudation in the Altai, given the more proximal location of the Altai to the Mongol-Okhotsk collision zone. The widespread Cretaceous AFT ages and late Mesozoic cooling episode obtained for the Ili-Balkhash basement ranges are hence compatible with previous thermo-tectonic studies in the adjoining area, and are interpreted in the same context, mainly as far-field effects of the Cimmerian collisions at the southern Eurasian margin and possibly also of the Mongol-

Okhotsk Orogeny in SE Siberia during the Jurassic-Cretaceous (Choulet et al., 2013; De Grave et al., 2007, 2013; Dumitru et al., 2001; Hendrix et al., 1992; Jolivet et al., 2013b) (Fig. 8). The variation in timing of the late Mesozoic cooling (and AFT ages) can be attributed to distinct tectonic movements and differences in exhumation rate and intensity between particular basement blocks.

In the Issyk-Kul Basin, the Mesozoic sedimentary record contains a few hundred meters of Upper Triassic - Jurassic sediments and minor Cretaceous deposits (Cobbold et al., 1994), while in the southern Junggar Basin, the Mesozoic sedimentary pile is thicker and ends with Cretaceous coarse clastic sediments (Allen et al., 1995; Hendrix et al., 1992; Jolivet et al., 2010; Wang et al., 2013; Yang et al., 2015). Unfortunately, in the IBB, the Mesozoic sedimentary record is relatively poorly known, making direct correlation between the Mesozoic exhumation history and the resulting sediment supply not straightforward. However, the clear presence of Jurassic – Cretaceous sediments in the nearby area is consistent with the interpretation of late Mesozoic basement denudation. A lot of studies demonstrate that Mesozoic deformation in the Tien Shan and Altai was periodical (e.g. Dumitru et al., 2001; Glorie et al., 2011b, 2012b; Hendrix et al., 1992; Jolivet et al., 2010; Yang et al., 2015). For example, Choulet et al. (2013) correlated Mesozoic episodes of strike-slip faulting and coarse-grained detrital sedimentation in the South Junggar Basin with rotational movements between Kazakhstan, Junggar, Tarim and Siberia, which can be seen as effects of the Cimmerian collisions at the southern Eurasian margin. Therefore, the Mesozoic Tien Shan and Altai were probably characterized by localized, differential uplifted ranges and intervening basins. Because of the non-uniform and complex nature of the reactivation, direct correlation between the distant tectonic forces, the timing and distribution of the intracontinental deformation revealed by e.g. AFT dating and the sediment record is not always clear. Discrepancies between the sedimentological record and low-temperature thermochronological data in the Mesozoic are described by Jolivet et al. (2010) for the Chinese Ili Basin, and by Jolivet et al. (2013b) and Vincent and Allen (2001) for the Junggar Basin. Also, Jolivet et al. (2015) demonstrate that the link between tectonic uplift and the sediment record is often not straightforward, and can be considerably modified by climate variations

as in the case of the Upper Jurassic – Lower Cretaceous alluvial fan deposits of the Kalaza Formation for example.

5.2.2 Late Cretaceous – Paleogene tectonic stability

A slow cooling period from the latest Mesozoic through the Paleogene is clearly present in most THMs (Fig. 7), but some caution is needed to interpret this slow cooling phase because it often takes place at temperatures just outside the PAZ where the sensitivity of the model decreases. However, such a slow cooling period is also recognized in the thermochronological data from the northern Kyrgyz Tien Shan (Bullen et al., 2001, 2003; De Grave et al., 2013; Glorie et al., 2010; Macaulay et al., 2013, 2014) and southern Altai (De Grave and Van den haute, 2002; De Grave et al., 2008; Yuan et al., 2006).

Evidence for this tectonic stable period can also be found in the sedimentary record. In the IBB, the most complete sedimentary section is located south of the Aktau Mountains, situated southwest of the Kazakh West Junggar Range (Fig. 2 and 4). In this region, Cenozoic deposits rest unconformable on Upper Cretaceous sedimentary rocks (Lucas et al., 2000 and references therein). After the deposition of scattered Cretaceous sediments in the IBB and adjoining basins, a regionally extensive peneplain developed. Remnants of these flat erosional surfaces can be found in the Tien Shan and Altai (Allen et al., 2001; De Grave and Van den haute, 2002; Sobel et al., 2006 and references therein). In the IBB, sedimentation resumed during the late Eocene – Oligocene, and became widespread since the early Miocene (Kober et al., 2013; Lucas et al., 1997, 2000). During the late Eocene - early Miocene the deposits were mainly fluvio-lacustrine in origin and reflect distal, low-energy sedimentary environments (Kober et al., 2013; Lucas et al., 1997, 2000). Comparable to the IBB, the adjacent Chu Basin contains ± 6 km of Cenozoic sediments, resting on Cretaceous deposits (Bullen et al., 2001 and references therein). The relative thin Cretaceous - Paleogene strata probably represent low-energy environment sediments, whereas a transition to more fluvial-alluvial sedimentary settings progressed during the Miocene (Bullen et al., 2001). In the Junggar Basin, also

limited erosion and associated sedimentation took place during the Paleogene (Wang et al., 2001). Hence, the near lack of sedimentary deposits during the Paleogene in the IBB and adjoining basins is in agreement with the slow basement cooling episode derived from our AFT data.

5.2.3 Late Cenozoic reactivation

A late Cenozoic cooling phase might be present in some of the THMs, but is only clearly outspoken in the model of sample 11-28 (Fig. 7). Very precise timing of this cooling phase is difficult because most samples were almost at near-surface temperatures at that time, where the sensitivity of the AFT method is decreasing. Therefore, this event is less outspoken as compared to the late Mesozoic cooling. For some samples (e.g. SK-32, Fig. 7) late Cenozoic cooling is lacking because these samples were already brought to ambient surface conditions by the late Mesozoic – early Cenozoic. However, the late Cenozoic cooling event is obviously most pronounced in samples 11-27 and 11-28 from the Trans-Ili Range, which reveal Miocene AFT ages (respectively 10.1 (± 0.6) and 16.8 (± 0.8) Ma) (Fig. 6 and 8, Table 4). The THM of sample 11-28 shows a distinct cooling-exhumation phase from below the APAZ to ambient surface conditions during the late Cenozoic (Fig. 7 and 8). Such a late Cenozoic cooling phase is widely recognized in the Tien Shan and reflects the onset of modern mountain building and associated basement denudation related to the ongoing indentation of the Indian plate into Eurasia. Although some major structures in the Tien Shan have been reactivated since the early Eocene (e.g. Glorie et al., 2011b), the building of the modern Tien Shan is generally believed to have started in the Oligocene - early Miocene, and exhumation was widespread from the Miocene onwards (e.g. Bullen et al., 2001, 2003; Buslov et al., 2008; De Grave et al., 2013; Jolivet et al., 2010; Macaulay et al., 2013, 2014; Sobel and Dumitru, 1997; Sobel et al., 2006; Yu et al., 2014). For example, Bullen et al. (2001) reported AFT ages between 20 and 10 Ma for the Kyrgyz Range, in the northern Kyrgyz Tien Shan. Also De Grave et al. (2013) and Macaulay et al. (2014) confirmed that in the Kyrgyz northern Tien Shan increased exhumation occurred between 15 and 5 Ma, and that the mountain ranges south of the Issyk Kul Basin deformed out-of-sequence, related to inherited

structural weak zones. Magnetostratigraphic studies also underscore that the onset of the development of the modern Tien Shan initiated during the Miocene (Charreau et al., 2006, 2009). In the Altai region, late Cenozoic reactivation seems to start in the Miocene, with clear intensification in the Pliocene, and reflects in an analogous manner the initiation of the construction of the modern Altai Mountains (De Grave and Van den haute, 2002; Vassallo et al., 2007; Yuan et al., 2006).

After a period of minor sedimentation during the Paleogene, coarser clastic and thicker sedimentary piles are recognized since the Mio - Pliocene in the Junggar, Issyk-Kul and Chu basins (Cobbold et al., 1993; De Grave et al., 2013; Wang et al. 2001, 2009b). Likewise, in the IBB, sedimentation became more widespread since the Neogene (Kober et al., 2013; Lucas et al., 1997, 2000). During the middle Miocene, a large lake/playa system existed in the center of the IBB (Kober et al., 2013). Up to then, sedimentation in the IBB was accompanied by local normal faulting. These normal faults became reactivated as reverse or strike-slip faults since the middle - late Miocene (Kober et al., 2013). Since the Plio – Pleistocene, coarser detrital sediments are deposited in the IBB (Kober et al., 2013; Lucas et al., 1997, 2000). Our AFT results are in agreement with these findings and confirm that more shortening and deformation took place in the IBB since the Miocene.

A topographic profile from Almaty (SE Kazakhstan) to Cholpon-Ata (NE Kyrgyzstan), crosscutting the Trans-Ili and Kungey Ranges, is given in Fig. 9. AFT data shown for this transect is based partly on samples from De Grave et al. (2013) (ALMA03-1/2/3, TS-04, TS-06 to TS-12), and partly on samples from this study (11-27, 11-28). The ALMA03-1/2/3 samples at the northern side of the Trans-Ili Range show a normal age-elevation relationship, with AFT ages ranging from 71 to 23 Ma. Samples TS-06 to TS-12 at the southern flank of the Kungey Range also show a normal age-elevation relationship, but AFT ages now range from 147 to 116 Ma (De Grave et al., 2013). This age-offset between the two groups of samples is probably linked to the existence of active E-W oriented faults (Abdrakhmatov et al., 2002; Buslov et al., 2003a; Delvaux et al., 2001, 2013; Selander et al., 2012; Torizin et al., 2009) (Fig. 2, 6 and 9). Samples 11-27 and 11-28 - with Miocene AFT ages - are

located close to the Trans-Ili or Zailisky Fault (ZF), which merge with the Chon-Kemin-Chilik Fault (CKCF) at depth (Delvaux et al., 2001; Torizin et al., 2009). Based on the seismic density map of Torizin et al. (2009), most seismicity in the Trans-Ili Range occurs around the Trans-Ili Fault (ZF), followed by the Karakunug-Almaty Fault (KAF) and the CKCF respectively, whereas south of the CKCF, in the Kungey Range, the seismic activity is less outspoken (Fig. 9). The ALMA03-1/2/3, 11-27 and 11-28 samples are located in this high seismicity zone, close to where the largest seismic events of the region occurred (Verny earthquake in 1887 (M = 7.3); Kemin earthquake in 1911 (M = 8.2)) (Abdrakhmatov et al., 2002, Delvaux et al., 2001; Torizin et al., 2009) (Fig. 9). Hence, late Cenozoic fault activity is probably responsible for the rapid and intense basement denudation, resulting in Miocene AFT ages in close vicinity of the ZF and KAF systems (Fig. 9). In comparison, in the Terskey Range, south of the Issyk-Kul Basin, a few similar late Oligocene to Miocene AFT ages are reported often in the vicinity of fault zones (De Grave et al., 2013; Macaulay et al., 2014). Furthermore, in the Chinese and southern Kyrgyz Tien Shan, similar Neogene AFT ages were documented in the vicinity of major E-W trending fault systems (e.g. Dumitru et al., 2001; Glorie et al., 2011b; Yang et al., 2014a). Hence, denudation in the late Cenozoic seems to be at least partially controlled by fault activity.

6 Conclusions

Based on the geo- and thermochronological results, the following conclusions can be drawn for the Ili-Balkhash basement of SE Kazakhstan:

(1) Eight magmatic basement samples reveal zircon U-Pb crystallization ages between ~350 and 260 Ma, spanning the Carboniferous to Permian time period. The Carboniferous (~350 - 320 Ma) crystallization ages can be related to subduction of the Junggar-Balkhash Ocean and subsequent building of the Balkhash-Ili magmatic belt, whereas the early (~296-297 Ma) and late (~258 Ma) Permian ages probably correspond to collisional and post-collisional magmatism in the context of the late Paleozoic final amalgamation of the ancestral Central Asian Orogenic Belt.

(2) Apatite fission track ages and thermal history models fit into the thermochronological framework of the adjoining Tien Shan and Altai regions. Since the final amalgamation of the ancestral CAOB in the Permian, the study area was subjected to late Mesozoic and late Cenozoic reactivation periods.

(3) The predominantly Cretaceous AFT ages and thermal history models of the Ili-Balkhash basement point to a distinct late Mesozoic cooling period associated with basement denudation. The Cimmerian collisions at the southern Eurasian margin and possibly the Mongol-Okhotsk Orogeny in SE Siberia are envisaged as main tectonic drives for this late Mesozoic reactivation period. The variation in timing of the late Mesozoic cooling paths (and AFT ages) can be attributed to distinct tectonic movements and differences in exhumation rate between particular basement blocks.

(4) After a late Mesozoic reactivation episode, a tectonic stable period is recognized in the AFT thermal history models (slow cooling paths) during the Paleogene. This is in agreement with the nearly lack of sedimentary deposits and development of a regional peneplain during the Paleogene in SE Kazakhstan and adjoining regions.

(5) Late Cenozoic AFT cooling started around the late Oligocene - Miocene and reflects the onset of modern mountain building and denudation in SE Kazakhstan. Along the active Trans-Ili Fault in the Kazakh Tien Shan, two Miocene AFT ages (~17 and 10 Ma) were obtained. This modern denudation is also expressed by the marked change towards coarser clastic sedimentary deposits in the area since the middle Miocene and can be explained as a far-field effect of the ongoing indentation of the Indian plate into Eurasia.

Acknowledgements

This research was supported by the DARIUS program. Stijn Glorie's contribution was supported by the Australian Research Council grant DP150101730 and forms TraX Record #307. We are indebted to Dr. Guido Vittiglio and Bart Van Houdt for their help with irradiations and neutron dosimetry at

the Belgian Nuclear Research Centre in Mol (SCK-CEN, BR1 facility) and to Dr. Vladislav Batalev and Prof. Dr. Neil Davies for their help during the field expedition. We are also very grateful to Ann-Eline Debeer for her assistance in our laboratory in Ghent. Reviews of the original manuscript by Dr. Marc Jolivet and Dr. Jiyuan Yin were very helpful and contributed to this final version of the manuscript.

References

Abdrakhmatov, K. Ye., Aldazhanov, S.A., Hager, B.H., Hamburger, M.W., Herring, T.A., Kalabaev, K.B., Makarov, V.I., Molnar, P., Panasyuk, S.V., Prilepin, M.T., Reilinger, R.E., Sadybakasov, I.S., Souter, B.J., Trapeznikov, Yu. A., Tsurkov, V. Ye., Zubovich, A.V. (1996). Relatively recent construction of the Tien Shan inferred from GPS measurements of present-day crustal deformation. Nature, 384, 450-453.

Abdrakhmatov, K.Y., Djanuzakov, K.D., Delvaux, D. (2002). Active tectonics and seizmic hazard of the Issyk-Kul basin in the Kyrgyz Tian-Shan. In: Klerkx, J., Imanackunov, B. (Eds). Lake Issyk-Kul: its natural environment. Kluwer Academic Publishers, Dordrecht, pp. 147-160.

Abrajevitch, A., Van der Voo, R., Levashova, N.M., Bazhenov, M.L. (2007). Paleomagnetic constraints on the paleogeography and oroclinal bending of the Devonian volcanic arc in Kazakhstan. Tectonophysics, 441, 67-84.

Abrajevitch, A., Van der Voo, R., Bazhenov, M.L., Levashova, N.M., McCausland, P.J.A. (2008). The role of the Kazakhstan orocline in the late Paleozoic amalgamation of Eurasia. Tectonophysics, 455, 61-76.

Alexeiev, D. V., Ryazantsev, A. V., Kröner, A., Tretaykov, A. A., Xia, X., Liu, D. Y. (2011) Geochemical data and zircon ages for rocks in a high-pressure belt of Chu-Yili Mountains, southern Kazakhstan: Implications for the earliest stages of accretion in Kazakhstan and the Tienshan. Journal of Asian Earth Sciences, 42, 805-820.

Allen, M.B., Şengör, A.M.C., Natal'in, B.A. (1995). Junggar, Turfan and Alakol basins as Late Permian to Early Triassic extensional structures in a sinistral shear zone in the Altaid orogenic collage, Central Asia. Journal of the Geological Society, London, 152(2), 327-338.

Allen, M.B., Alsop, G.I., Zhemchuzhnikov, V.G. (2001). Dome and basin refolding and transpressive inversion along the Karatau fault System, southern Kazakstan. Journal of the Geological Society, London, 158, 83-95.

Barbarand, J., Carter, A., Wood, I., Hurford, T. (2003) Compositional and structural control of fission-track annealing in apatite. Chemical Geology, 198, 107-137.

Bazhenov, M. L., Levashova, N. M., Degtyarev, K. E., Van der Voo, R., Abrajevitch, A. V., McCausland, P. J. A. (2012). Unraveling the early-middle Paleozoic paleogeography of Kazakhstan on the basis of Ordovician and Devonian paleomagnetic results. Gondwana Research, 22, 974-991.

Biske, Y. S., Konopelko, D. L., Seltmann, R. (2013). Geodynamics of Late Paleozoic Magmatism in the Tien Shan and Its Framework. Geotectonics, 47, 291-309.

Bullen, M.E., Burbank, D.W., Garver, J.I., Abdrakhmatov, K. Ye. (2001). Late Cenozoic tectonic evolution of the northwestern Tien Shan: New age estimates for the initiation of mountain building. GSA Bulletin, 113(12), 1544-1559.

Bullen, M. E., Burbank, D. W., Garver, J. I. (2003). Building the Northern Tien Shan: Integrated thermal, structural, and topographic constraints. Journal of Geology, 111(2), 149-165.

Buslov, M.M. (2011). Tectonics and geodynamics of the Central Asian Foldbelt: the role of Late Paleozoic large-amplitude strike-slip faults. Russian Geology and Geophysics, 52, 52–71.

Buslov, M. M., Klerkx, J., Abdrakhmatov, K., Delvaux, D., Batalev, V. Y., Kuchai, O. A., Dehandschutter, B., Muraliev, A. (2003a). Recent strike-slip deformation of the northern Tien Shan. In: Storti, F., Holdsworth, R. E., Salvini, F. (Eds.). Intraplate strike-slip deformation belts. Geological Society, London, Special Publications, 210, 53-64.

Buslov, M.M., Watanabe, T., Smirnova, L.V., Fujiwara, I., Iwata, K., De Grave, J., Semakov, N.N., Travin, A.V., Kir'yanova, A.P., Kokh, D.A. (2003b). Role of strike-slip faulting in Late Paleozoic – Early Mesozoic tectonics and geodynamics of the Altai-Sayan and East Kazashstan Regions. Russian Geology and Geophysics, 44, 49-75.

Buslov, M.M., Watanabe, T., Fujiwara, Y., Iwata, K., Smirnova, L.V., Safonova, I.Yu., Semakov, N.N., Kiryanova, A.P. (2004). Late Paleozoic faults of the Altai region, Central Asia: tectonic pattern and model of formation. Journal of Asian Earth Sciences, 23, 655–671.

Buslov, M. M., De Grave, J., Bataleva, E. A. V., Batalev, V. Y. (2007). Cenozoic tectonic and geodynamic evolution of the Kyrgyz Tien Shan Mountains: A review of geological, thermochronological and geophysical data. Journal of Asian Earth Sciences, 29, 205-214.

Buslov, M. M., Kokh, D. A., De Grave, J. (2008). Mesozoic-Cenozoic tectonics and geodynamics of Altai, Tien Shan, and Northern Kazakhstan, from apatite fission-track data. Russian Geology and Geophysics, 49, 648-654.

Buslov, M.M., Geng, H., Travin, A.V., Otgonbaatar, D., Kulikova, A.V., Chen, M., Glorie , S., Semakov, N.N., Rubanova, E.S., Abildaeva, M.A., Voitishek, E.E., Trofimova, D.A. (2013). Tectonics and geodynamics of Gorny Altai and adjacent structures of the Altai–Sayan folded area. Russian Geology and Geophysics, 54, 1250-1271.

Campbell, G. E., Walker, R. T., Abdrakhmatov, K., Schwenninger, JL., Jackson, J., Elliott, J. R., Copley, A. (2013). The Dzhungarian fault: Late Quaternary tectonics and slip rate of a major right-lateral strike-slip fault in the northern Tien Shan region. Journal of Geophysical Research: solid earth, 118, 5681-5698.

Carlson, W. D., Donelick, R. A., Ketcham, R. A. (1999). Variability of apatite fission-track annealing kinetics: I. Experimental results. American Mineralogist, 84, 1213-1223.

Charreau, J., Gilder, S., Chen, Y., Dominguez, S., Avouac, J.-P., Sen, S., Jolivet, M., Li, Y., Wang, W. (2006). Magnetostratigraphy of the Yaha section, Tarim basin (China): 11 Ma acceleration in erosion and uplift of the Tianshan Mountains. Geology, 34(3), 181-184.

Charreau, J., Chen, Y., Gilder, S., Barrier, L., Dominguez, S., Augier, R., Sen, S., Avouac, J-P., Gallaud, A., Graveleau, F., Wang, Q. (2009). Neogene uplift of the Tien Shan Mountains observed in the magnetic record of the Jingou River section (northwest China). Tectonics, 28, TC2008.

Charvet, J., Shu, L., Laurent-Charvet, S. (2007). Paleozoic structural and geodynamic evolution of eastern Tianshan (NW China): welding of the Tarim and Junggar plates. Episodes, 30, 162-186.

Chen, B., Jahn, B.-M. (2004). Genesis of post-collisional granitoids and basement nature of the Junggar Terrane, NW China: Nd–Sr isotope and trace element evidence. Journal of Asian Earth Sciences, 23, 691-703.

Chen, X., Qu, W., Han, S., Eleonora, S., Yang, N., Chen, Z., Zeng, F., Du, A., Wang, Z. (2010). Re-Os geochronology of Cu and W-Mo deposits in the Balkhash metallogenic belt, Kazakhstan and its geological significance. Geoscience Frontiers, 1, 115-124.

Chen, X. H., Wang, Z.H., Chen, Z.L., Han, S. Q., Seitmuratova, E., Yang, Y., Ye, B. Y., Chen W. (2012). Geochronological constraints on skarn copper metallogenesis of the large-scale Sayak ore field, Kazakhstan, Central Asia. Acta Petrologica Sinica, 28,1981-1994. (in Chinese with English abstract).

Chen, X., Seitmuratova, E., Wang, Z., Chen, Z., Han, S., Li, Y., Yang, Y., Ye, B., Shi, W. (2014). SHRIMP U–Pb and Ar–Ar geochronology of major porphyry and skarn Cu deposits in the Balkhash Metallogenic Belt, Central Asia, and geological implications. Journal of Asian Earth Sciences, 79, 723-740.

Cherniak, D., Watson, E. (2003). Diffusion in Zircon. In: Hanchar, J., Hoskin, P. (Eds). Zircon. Reviews in Mineralogy and Geochemistry, 53, 113-139.

Choulet, F., Chen, Y., Wang, B., Faure, M., Cluzel, D., Charvet, J., Lin, W., Xu, B. (2011). Late Paleozoic paleogeographic reconstruction of Western Central Asia based upon paleomagnetic data and its geodynamic implications. Journal of Asian Earth Sciences, 42, 867-884.

Choulet, F., Faure, M., Cluzel, D., Chen, Y., Lin, W., Wang, B. (2012). From oblique accretion to transpression in the evolution of the Altaid collage: New insights from West Junggar, northwestern China. Gondwana Research, 21, 530-547.

Choulet, F., Chen, Y., Cogné, J. P., Rabillard, A., Wang, B., Lin, W., Faure, M., Cluzel, D. (2013). First Triassic palaeomagnetic constraints from Junggar (NW China) and their implications for the Mesozoic tectonics in Central Asia. Journal of Asian Earth Sciences, 78, 371-394.

Cobbold, P.R., Davy, P., Gapais, D., Rossello, E.A., Sadybakasov, E., Thomas, J.C., Tondji Biyo, J.J., de Urreiztieta, M. (1993). Sedimentary basins and crustal thickening. Sedimentary Geology, 86, 77-89.

Cobbold, P.R., Sadybakasov, E., Thomas, J.C. (1994). Cenozoic transpression and basin development, Kyrghyz Tienshan, Central Asia. In: Roure, F., Ellouz, N., Shein, V.S., Skvortsov, I. (Eds.), Geodynamic Evolution of Sedimentary Basins. International Symposium, Moscow, pp. 181–202.

Cogné, J.-P., Kravchinsky, V. A., Halim, N., Hankard, F. (2005). Late Jurassic-Early Cretaceous closure of the Mongol-Okhotsk Ocean demonstrated by new Mesozoic palaeomagnetic results from the Trans-Baïkal area (SE Siberia). Geophysical Journal International, 163, 813-832.

Corfu, F., Hanchar, J. M., Hoskin, P. W. O., Kinny, P. (2003). Atlas of Zircon Textures. Reviews in Mineralogy and Geochemistry, 53, 469-500.

De Corte, F., Bellemans, F., Van den haute P., Ingelbrecht, C., Nicholl, C. (1998). A new U doped glass certified by the European Commission for the calibration of fission-track dating. In: Van den haute, P. and De Corte, F. (Editors). Advances in fission-track geochronology, Kluwer Academic Publishers, Dordrecht, pp. 67-78

De Grave, J., Van den haute, P. (2002). Denudation and cooling of the Lake Teletskoye Region in the Altai Mountains (South Siberia) as revealed by apatite fission-track thermochronology. Tectonophysics, 349, 145-159.

De Grave, J., Buslov, M.M., Van den haute, P. (2007). Distant effects of India-Eurasia convergence and Mesozoic intracontinental deformation in Central Asia: Constraints from apatite fission-track thermochronology. Journal of Asian Earth Sciences, 29, 188-204.

De Grave, J., Van den haute, P., Buslov, M.M., Dehandschutter, B., Glorie, S. (2008). Apatite fission-track thermochronology applied to the Chulyshman Plateau, Siberian Altai Region. Radiation Measurements, 43, 38-42.

De Grave, J., Buslov, M.M., Van den haute, P., Metcalf, J., Dehandschutter, B., McWilliams, M.O. (2009). Multi-method chronometry of the Teletskoye graben and its basement, Siberian Altai Mountains: new insights on its thermo-tectonic evolution. From: Lisker, F., Ventura, B., Glasmacher, U.A. Thermochronological methods: From paleotemperature Constraints to Landscape evolution models. Geological Society, London, Special Publications, 324, 237-259.

De Grave, J., Glorie, S., Buslov, M.M., Izmer, A., Fournier-Carrie, A., Elburg, M., Batalev, V. Yu., Vanhaeke, F., Van den haute, P. (2011a). The thermo-tectonic history of the Song-Kul Plateau, Kyrgyz Tien Shan: constraints by apatite and titanite thermo-chronometry and zircon U/Pb dating. Gondwana Research, 20, 745-763.

De Grave, J., Glorie, S., Zhimulev, F.I., Buslov, M.M., Elburg, M., Vanhaecke, F., Van den haute, P. (2011b). Emplacement and exhumation of the Kuznetsk-Alatau basement (Siberia): implications for the tectonic evolution of the Central Asian Orogenic Belt and sediment supply to the Kuznetsk, Minusa and West Siberian Basins. Terra Nova, 23, 248-256.

De Grave, J., Glorie, S., Ryabinin, A., Zhimulev, F. Izmer, A., Buslov, M.M., Elburg, M., Vanhaeke, F., Van den haute, P. (2012). Late Palaeozoic and Meso-Cenozoic tectonic evolution of the Southern Kyrgyz Tien Shan: constraints from multi-method thermochronology in the Trans-Alai, Turkestan-Alai Section and the Southeastern Ferghana Basin. Journal of Asian Earth Sciences, 44, 149-168.

De Grave, J. , Glorie, S., Buslov, M.M., Stockli, D.F., McWilliams, M.O., Batalev, V. Y., Van den haute P. (2013). Thermo-tectonic history of the Issyk-Kul basement (Kyrgyz Northern Tien Shan, Central Asia). Gondwana Research, 23, 998-1020.

Degtyarev, K. E. (2011). Tectonic Evolution of Early Paleozoic Island-Arc Systems and Continental Crust Formation in the Caledonides of Kazakhstan and the North Tien Shan. Geotectonics, 45, 23-50.

Degtyarev, K. E., Shatagin, K. N., Kotov, A. B., Sal'nikova, E. B., Luchitskaya, M. V., Yakovleva, S. Z., Plotkina, YU. V., Fedoseenko, A. M. (2006). Early Paleozoic Granitoids of the Aqtau–Dzungar Microcontinent (Central Kazakhstan). Doklady Earth Sciences, 411, 1204-1208.

Delvaux, D., Abdrakhmatov, K. E., Lemzin, I. N., Strom, A. L. (2001). Landslides and surface breaks of the 1911 M_s 8.2 Kemin earthquake (Kyrgyzstan). Russian Geology and Geophysics, 42, 1583-1592.

Delvaux, D., Cloetingh, S., Beekman, F., Sokoutis, D., Burov, E., Buslov, M.M., Abdrakhmatov, K.E. (2013). Basin evolution in a folding lithosphere: Altai-Sayan and Tien Shan belts in Central Asia. Tectonophysics, 602, 194-222.

Dobretsov, N. L. (2011). Early Paleozoic tectonics and geodynamics of Central Asia: role of mantle plumes. Russian Geology and Geophysics, 52, 1539-1552.

Dobretsov, N.L., Buslov, M.M. (2007). Late Cambrian–Ordovician tectonics and geodynamics of Central Asia. Russian Geology and Geophysics, 48, 71–82.

Donelick, R.A., Ketcham, R.A., Carlson, W.D. (1999). Variability of apatite fission-track annealing kinetics: II. Crystallographic orientation effects. American Mineralogist, 84(9), 1224-1234.

Donelick, R., O'Sullivan, P., Ketcham, R. (2005). Apatite fission-track analysis. Reviews in Mineralogy and Geochemistry, 58, 49-94.

Dong, Y., Zhang, G., Neubauer, F., Liu, X., Hauzenberger, C., Zhou, D., Li, W. (2011). Syn- and post-collisional granitoids in the Central Tianshan orogen: Geochemistry, geochronology and implications for tectonic evolution. Gondwana Research, 20, 568-581.

Dumitru, T.A., Zhou, D., Chang, E.Z., Graham, S.A. (2001). Uplift, exhumation, and deformation in the Chinese Tian Shan. Geological Society of America Memoir, 194, 71–99.

Feng, Y., Coleman, R. G., Tilton, G., Xiao, X. (1989). Tectonic evolution of the West Junggar region, Xinjiang, China. Tectonics, 8, 729-752.

Filippova, I.B., Bush, V.A., Didenko, A.N. (2001). Middle Paleozoic subduction belts: the leading factor in the formation of the Central Asian fold-and-thrust belt. Russian Journal of Earth Science, 3, 405-426.

Galbraith, R. F. (1990). The radial plot: graphical assessment of spread in ages. Nuclear Tracks and Radiation Measurements, 17, 207-214.

Gallagher, K. (2012). Transdimensional inverse thermal history modeling for quantitative thermochronology. Journal of Geophysical Research: Solid Earth, 117 (B2).

Gao, R., Xiao, L., Pirajno, F., Wang, G.-C., He, X.-X., Yang, G., Yan, S.-W. (2014). Carboniferous-Permian extensive magmatism in the West Junggar, Xinjiang, northwestern China: its geochemistry, geochronology, and petrogenesis. Lithos, 204, 125-143.

Geng, H., Sun, M., Yuan, C., Xiao, W., Xian, W., Zhao, G., Zhang, L., Wong, K., Wu, F. (2009). Geochemical, Sr-Nd and zircon U-Pb-Hf isotopic studies of Late Carboniferous magmatism in the West Junggar, Xinjiang: Implications for ridge subduction? Chemical Geology, 266, 364-389.

Geng, H., Sun, M., Yuan, C., Zhao, G., Xiao, W. (2011). Geochemical and geochronological study of early Carboniferous volcanic rocks from the West Junggar: Petrogenesis and tectonic implications. Journal of Asian Earth Sciences, 42, 854-866.

Gleadow, A.J.W., Duddy, I.R., Green, P.F., Lovering, J.F. (1986). Confined fission track lengths in apatite: a diagnostic tool for thermal history analysis. Contributions to Mineralogy and Petrology, 94, 405-415.

Glorie, S., De Grave, J. (2015). Exhuming the Meso-Cenozoic Kyrgyz Tian Shan and Siberian Altai-Sayan: a review based on low-temperature thermochronology. Geoscience Frontiers, in press.

Glorie, S., De Grave, J., Buslov, M.M., Elburg, M.A., Stockli, D.F., Gerdes, A., Van den haute, P. (2010). Multi-method chronometric constraints on the evolution of the Northern Kyrgyz Tien Shan granitoids

(Central Asian Orogenic Belt): From emplacement to exhumation. Journal of Asian Earth Sciences, 38, 131-146.

Glorie, S., De Grave, J., Buslov, M.M., Zhimulev, F.I., Izmer, A., Vandoorne, W., Ryabinin, A., Van den haute, P., Vanhaecke, F., Elburg, M. (2011a). Formation and Palaeozoic evolution of the Gorny-Altai - Altai-Mongolia suture zone (South Siberia): zircon U/Pb constraints on its igneous record. Gondwana Research, 20, 465-484.

Glorie, S., De Grave, J., Buslov, M.M., Zhimulev, F.I., Stockli, D.F., Batalev, V.Yu., Izmer, A., Van den haute, P., Vanhaecke, F., Elburg, M.A. (2011b). Thermotectonic history of the Kyrgyz South Tien Shan (Atbashi-Inylchek) suture zone: the role of inherited structures during deformation-propagation. Tectonics, 30, TC6016.

Glorie, S., De Grave, J., Buslov, M.M., Zhimulev, F.I., Elburg, M.A., Van den haute, P. (2012a). Structural control on Meso-Cenozoic tectonic reactivation and denudation in the Siberian Altai: Insights from multi-method thermochronometry. Tectonophysics, 544-545, 75-92.

Glorie, S., De Grave, J., Delvaux, D., Buslov, M.M., Zhimulev, F.I., Van den haute, P. (2012b). Tectonic history of the Irtysh shear zone (NE Kazakhstan): new constraints from zircon U/Pb dating, apatite fission track dating and paleostress analysis. Journal of Asian Earth Sciences, 45, 138-149.

Glorie, S., Zhimulev, F. I., Buslov, M.M., Andersen, T., Plavsa, D., Izmer, A., Vanhaecke, F., De Grave, J. (2015). Formation of the Kokchetav subduction–collision zone (northern Kazakhstan): Insights from zircon U–Pb and Lu–Hf isotope systematics. Gondwana Research, 27, 424-438.

Golonka, J. (2004). Plate tectonic evolution of the southern margin of Eurasia in the Mesozoic and Cenozoic. Tectonophysics, 381, 235-273.

Green, P. F., Duddy, I. R., Gleadow, A. J. W., Tingate, P. R., Laslett, G. M. (1986). Thermal annealing of fission tracks in apatite 1.A qualitative description. Chemical Geology, 59, 237-253.

Guo, L. S., Liu, Y.L., Wang, Z. H., Song, D., Xu, F.J., Su, L. (2010). The zircon U-Pb LA-ICP-MS geochronology of volcanic rocks in Baogutu areas, western Junggar. Acta Petrologica Sinica, 26, 471-477 (in Chinese with English abstract).

Halim, N., Cogné, J. P., Chen, Y., Atasiei, R., Besse, J., Courtillot, V., Gilder, S., Marcoux, J. Zhao, R. L. (1998). New Cretaceous and Early Tertiary paleomagnetic results from Xining-Lanzhou basin, Kunlun and Qiangtang blocks, China: Implications on the geodynamic evolution of Asia. Journal of Geophysical Research, 103, 025-045.

Han, B.F., Ji, J.Q., Song, B., Chen, L.H., Zhang, L. (2006). Late Paleozoic vertical growth of continental crust around the Junggar Basin, Xinjiang, China (Part I): Timing of post-collisional plutonism. Acta Petrologica Sinica, 22, 1077-1086.

Han, B.-F., Guo, Z.-J., Zhang, Z.-C., Zhang, L., Chen, J.-f., Song, B. (2010). Age, geochemistry, and tectonic implications of a late Paleozoic stitching pluton in the North Tian Shan suture zone, western China. Geological Society of America Bulletin, 122, 627-640.

Han, B.-F., He, G.-Q., Wang, X.-C., Guo, Z.-J. (2011). Late Carboniferous collision between the Tarim and Kazakhstan–Yili terranes in the western segment of the South Tian Shan Orogen, Central Asia, and implications for the Northern Xinjiang, western China. Earth-Science Reviews, 109, 74-93.

Heinhorst, J., Lehmann, B., Ermolov, P., Serykh, V., Zhurutin, S. (2000). Paleozoic crustal growth and metallogeny of Central Asia: evidence from magmatic-hydrothermal ore systems of Central Kazakhstan. Tectonophysics, 328, 69-87.

Hendrix, M. S., Graham, S. A., Carroll, A. R., Sobel, E. R., McKnight, C. L., Schulein, B. J., Wang, Z. (1992). Sedimentary record and climatic implications of recurrent deformation in the Tien Shan: Evidence from Mesozoic strata of the north Tarim, south Junggar, and Turpan basins, Northwest China. Geological Society of America Bulletin, 104(1), 53-79.

Hendrix, M.S., Dumitru, T.A., Graham, S.A. (1994). Late Oligocene – Early Miocene unroofing in the Chinese Tien Shan – an early effect of the India-Asian collision. Geology 22, 487-490.

Hoskin, P. W. O. (2000). Patterns of chaos: fractal statistics and the oscillatory chemistry of zircon. Geochimica et Cosmochimica Acta, 64, 1905-1923.

Hurford, A.J. 1990. Standardization of fission track dating calibration: Recommendation by the Fission Track Working Group of the I.U.G.S. Subcommission on Geochronology. Chemical Geology (Isotope Geoscience Section), 80, 171-178.

Institute of Geology, Chinese Academy of Geological Sciences (IGCAGS) (2006) 1:2 500 000 Geological Map of Western China and adjacent regions. Geological Publishing House, Beijing (in Chinese). Chief compiler: Li Tingdong.

Jackson, S.E., Pearson, N.J., Griffin, W.L., Belousova, E. (2004). The application of laser ablation inductively coupled plasma mass spectrometry to in-situ U-Pb zircon geochronology. Chemical Geology, 211, 47-69.

Jolivet, M. (2015). Mesozoic tectonic and topographic evolution of Central Asia and Tibet: a preliminary synthesis. Geological Society of London Special Publication, in press.

Jolivet, M., Dominguez, S., Charreau, J., Chen, Y., Li, Y.G., Wang, Q.C. (2010). Mesozoic and Cenozoic tectonic history of the central Chinese Tian Shan: reactivated tectonic structures and active deformation. Tectonics, 29, TC6019.

Jolivet, M., Arzhannikov, S., Arzhannikova, A., Chauvet, A., Vassallo, R., Braucher, R. (2013a). Geomorphic Mesozoic and Cenozoic evolution in the Oka-Jombolok region (East Sayan ranges, Siberia). Journal of Asian Earth Sciences, 62, 117-132.

Jolivet, M., Heilbronn, G., Robin, C., Barrier, L., Bourquin, S., Guo, Zh., Jia, Y., Guerit, L., Yang, W., Fu, B. (2013b). Reconstructing the Late Palaeozoic – Mesozoic topographic evolution of the Chinese Tian Shan: available data and remaining uncertainties. Advances in Geosciences, 1, 1-12.

Jolivet, M., Bourquin, S., Heilbronn, G., Robin, C., Barrier, L., Dabard, M.-P., Jia, Y., De Pelsmaeker, E., Fu, B. (2015). The Upper Jurassic – Lower Cretaceous alluvial fan deposits of the Kalaza Formation (Central Asia): tectonic pulse or increased aridity? Geological Society of London Special Publication, in press.

Kapp, P., Murphy, M. A., Yin, A., Harrison, T. M., Ding, L., Guo, J. (2003). Mesozoic and Cenozoic tectonic evolution of the Shiquanhe area of western Tibet. Tectonics, 22, p 1029.

Ketcham, R.A. (2005). Forward and inverse modeling of low-temperature thermochronometry data. Reviews in Mineralogy and Geochemistry, 58, 275-314.

Ketcham, R.A., Donelick, R.A., Carlson, W.D. (1999). Variability of apatite fission-track annealing kinetics: III. Extrapolation to geological time scales. American Mineralogist, 84(9), 1235-1255.

Ketcham, R.A., Donelick, R.A., Donelick, M.B. (2000). AFTSolve: a program from multi-kinetic modeling of apatite fission-track data. Geological Materials Research, 2, 1-32.

Ketcham, R.A., Carter, A., Donelick, R.A., Barbarand, J., Hurford, A.J. (2007). Improved modeling of fission-track annealing in apatite. American Mineralogist, 92, 799-810.

Kober, M., Seib, N., Kley, J., Voigt, T. (2013). Thick-skinned thrusting in the northern Tien Shan foreland, Kazakhstan: structural inheritance and polyphase deformation. Geological Society, London, Special Publications, 377, SP377.7.

Konopelko, D., Biske, G., Seltmann, R., Eklund, O., Belyatsky, B. (2007). Hercynian post-collisional A-type granites of the Kokshaal Range, Southern Tien Shan, Kyrgyzstan. Lithos, 97, 140-160.

Korobkin, V.V., Buslov, M.M. (2011). Tectonics and geodynamics of the western Central Asian Fold Belt (Kazakhstan Paleozoides). Russian Geology and Geophysics, 52, 1600-1618.

Kröner, A., Hegner, E., Lehmann, B., Heinhorst, J., Wingate, M.T.D., Liu, D.Y., Ermelov, P. (2008). Palaeozoic arc magmatism in the Central Asian Orogenic Beld of Kazakhstan: SHRIMP zircon ages and whole-rock Nd isotopic systematics. Journal of Asian Earth Sciences, 32, 118-130.

Kröner, A., Alexeiev, D. V., Rojas-Agramonte, Y., Hegner, E., Wong, J. Xia, X., Belousova, E., Mikolaichuk, A. V., Seltmann, R., Liu, D., Kiselev, V. V. (2013) Mesoproterozoic (Grenville-age) terranes in the Kyrgyz North Tianshan: Zircon ages and Nd–Hf isotopic constraints on the origin and evolution of basement blocks in the southern Central Asian Orogen. Gondwana Research, 23, 272-295.

Levashova, N.M., Mikolaichuk, A.V., McCausland, P.J.A., Bazhenov, M.L., Van der Voo, R. (2007). Devonian paleomagnetism of the North Tien Shan: implications for the middle-Late Paleozoic paleogeography of Eurasia. Earth and Planetary Science Letters, 257, 104-120.

Levashova, N. M., Degtyarev, K. E., Bazhenov, M. L. (2012). Oroclinal Bending of the Middle and Late Paleozoic Volcanic Belts in Kazakhstan: Paleomagnetic Evidence and Geological Implications. Geotectonics, 46, 285-302.

Li, L., Chen, Z.L., Qi, W.X., Wang, S.X., Chen, X.H., Wu, Y.P., Gong, H.L., Wei, X.C., Yang, Y. Li, X.Z. (2008). Apatite fission track evidence for uplifting-exhumation processes of mountains surrounding the Junggar basin. Acta Petrologica Sinica, 24, 1011-1020. (In Chinese with English abstract).

Li, G.-M., Cao, M.-J., Qin, K.-Z., Evans, N. J., McInnes, B.I.A., Liu, Y.-S. (2014). Thermal-tectonic history of the Baogutu porphyry Cu deposit, West Junggar as constrained from zircon U-Pb, biotite Ar/Ar and zircon/apatite (U-Th)/He dating. Journal of Asian Earth Sciences, 79, 741-758.

Liu, D., Guo, Z., Jolivet, M., Cheng, F., Song, Y., Zhang, Z. (2014). Petrology and geochemistry of Early Permian volcanic rocks in South Tian Shan, NW China: implications for the tectonic evolution and Phanerozoic continental growth. International Journal of Earth Sciences, 103, 737-756.

Lucas, S. G., Bayshashov, B. U., Tyutkova, L. A., Zhamangara, A. K., Aubekerov, B. Z. (1997). Mammalian biochronology of the Paleogene-Neogene boundary at Aktau Mountain, eastern Kazakhstan. Paläontologische Zeitschrift, 71, 305-314.

Lucas, S. G., Aubekerov, B. Z., Dzhamangaraeva, A. K., Bayshashov, B. U., Tyutkova, L. A. (2000). Cenozoic lacustrine deposits of the Ili Basin, southeastern Kazakhstan. In: Kelts, K. R. (ed.) Lake Basins Through Space and Time. American Association of Petroleum Geologists, Tulsa, 59-64.

Ludwig, K., 2003. User's Manual for Isoplot 3.00, A Geochronological Toolkit for Microsoft Excel. Berkeley Geochronology Center Special Publication v. 4.

Macaulay, E. A., Sobel E. R., Mikolaichuk, A., Landgraf, A., Kohn, B., Stuart, F. (2013). Thermochronologic insights into Late Cenozoic deformation in the basement-cored Terskey Range Kyrgyz Tien Shan. Tectonics, 32, 487-500.

Macaulay, E. A., Sobel E. R., Mikolaichuk, A., Kohn, B., Stuart, F. M. (2014). Cenozoic deformation and exhumation history of the Central Kyrgyz Tien Shan. Tectonics, 33, 135-165.

Metcalfe, I. (2013). Gondwana dispersion and Asian accretion: Tectonic and palaeogeographic evolution of eastern Tethys. Journal of Asian Earth Sciences, 66, 1-33.

Metelkin, D.V, Vernikovsky, V.A., Kazansky, A. Y., Wingate, M.T.D. (2010). Late Mesozoic tectonics of Central Asia based on paleomagnetic evidence. Gondwana Research, 18, 400-419.

Metelkin, D. V., Vernikovsky, V. A., Kazansky, A. Yu. (2012). Tectonic evolution of the Siberian paleocontinent from the Neoproterozoic to the Late Mesozoic: paleomagnetic record and reconstructions. Russian Geology and Geophysics, 53, 675-688.

Novikov, I. S. (2013). Reconstructing the stages of orogeny around the Junggar basin from the lithostratigraphy of Late Paleozoic, Mesozoic and Cenozoic sediments. Russian Geology and Geophysics, 54, 138 – 152.

Rolland, Y., Alexeiev, D., Kröner, A., Corsini, M., Loury, C., Monié, P. (2013). Late Palaeozoic to Mesozoic kinematic history of the Talas–Ferghana strike-slip fault (Kyrgyz West Tianshan) as revealed by $^{40}Ar/^{39}Ar$ dating of syn-kinematic white mica. Journal of Asian Earth Sciences, 67-68, 76-92.

Ren, R., Han, B.-F., Ji, J.-Q., Zhang, L., Xu, Z., Su, L. (2011). U–Pb age of detrital zircons from the Tekes River, Xinjiang, China, and implications for tectonomagmatic evolution of the South Tian Shan Orogen. Gondwana Research, 19, 460-470.

Roger, F., Jolivet, M., Malavieille, J. (2010). The tectonic evolution of the Songpan-Garzê (North Tibet) and adjacent areas from Proterozoic to Present: A synthesis. Journal of Asian Earth Sciences, 39, 254-269.

Selander, J., Oskin, M., Ormukov, C., Abdrakhmatov, K. (2012). Inherited strike-slip faults as an origin for basement-cored uplifts: Example of the Kungey and Zailiskey Ranges, northern Tian Shan. Tectonics, 31, TC4026.

Seltmann, R., Konopelko, D., Biske, G., Divaev, F., Sergeev, S. (2011). Hercynian post-collisional magmatism in the context of Paleozoic magmatic evolution of the Tien Shan orogenic belt. Journal of Asian Earth Sciences, 42, 821-838.

Sengör, A.M.C., Natal'in, B.A. (1996). Paleotectonics of Asia: fragments of a synthesis. In: Yin, A., Harrison, T.M. (Eds.). The tectonic Evolution of Asia. Cambridge University Press, New York, 486-641.

Sengör, A.M.C., Natal'in, B.A., Burtman, V.S. (1993). Evolution of the Altaid Tectonic Collage and Paleozoic Crustal Growth in Eurasia. Nature, 364(6435), 299-307.

Shen, P., Shen, Y., Li, X.-H., Pan, H., Zhu, H., Meng, L., Dai, H. (2012). Northwestern Junggar Basin, Xiemisitai Mountains, China: A geochemical and geochronological approach. Lithos, 140-141, 103-118.

Shen, P., Pan, H., Xiao, W., Chen, X., Seitmuratova, E., Shen, Y. (2013a). Two geodynamic – metallogenic events in the Balkhash (Kazakhstan) and the West Junggar (China): Carboniferous porphyry Cu and Permian greisen W-Mo mineralization. International Geology Review, 55, 1660 – 1687.

Shen, P., Xiao, W., Pan, H., Dong, L., Li, C. (2013b). Petrogenesis and tectonic settings of the Late Carboniferous Jiamantieliek and Baogutu ore-bearing porphyry intrusions in the southern West Junggar, NW China. Journal of Asian Earth Sciences, 75, 158-173.

Sláma, J., Kosler, D., Condon, D.J., Crowley, J.L., Gerdes, A., Hanchar, J.M., Horstwood, M.S.A., Morris, G.A., Nasdala, L., Norberg, N., Schaltegger, U., Schoene, B., Tubrett, M.N., Whitehouse, M.J. (2008). Plesovice zircon – a new natural reference material for U-Pb and Hf isotopic microanalysis. Chemical Geology, 249, 1-35.

Sobel, E.R., Dumitru, T.A. (1997). Thrusting and exhumation around the margins of the western Tarim basin during the India-Asia collision. Journal of Geophysical Research, 102, 5043-5063.

Sobel, E.R., Oskin, M., Burbank, D., Mikolaichuk, A. (2006). Exhumation of basement-cored uplifts: example of the Kyrgyz Range quantified with apatite fission track thermochronology. Tectonics, 25, TC2008.

Steiger, R.H., Jäger, E. (1977). Subcommission on geochronology: convention on the use of decay constants in geo- and cosmochronology. Earth and Planetary Science Letters, 36, 359-362.

Tang, G.-J., Wang, Q., Wyman, D., Sun, M., Li, Z.-X., Zhao, Z.-H., Sun, W.-D., Jia, X.-H., Jiang, Z.-Q. (2010). Geochronology and geochemistry of Late Paleozoic magmatic rocks in the Lamasu-Dabate area, northwestern Tianshan (west China): Evidence for a tectonic transition from arc to post-collisional setting. Lithos, 119, 393-411.

Thomas, J.C., Cobbold, P.R., Shein, V.S., Le Douaran, S. (1999). Sedimentary record of late Paleozoic to Recent tectonism in Central Asia – analysis of subsurface data from the Turan and Kazak domains. Tectonophysics, 313, 243-263.

Tong, Y., Wang, T., Jahn, B.-M., Sun, M., Hong, D.-W., Gao, J.-F. (2014). Post-accretionary Permian granitoids in the Chinese Altai Orogen: geochronology, petrogenesis and tectonic implications. American Journal of Science, 314, 80-109.

Torizin, J., Jentzsch, G., Malischewsky, P., Kley, J., Abakanov, N., Kurskeev, A. (2009). Rating of seismicity and reconstruction of the fault geometries in northern Tien Shan within the project "Seismic Hazard Assessment for Almaty". Journal of Geodynamics, 48, 269-278.

Van der Voo, R., Levashova, N.M., Skrinnik, L.I., Kara, T.V., Bazhenov, M.L. (2006). Late orogenic large-scale rotations in the Tien Shan and adjacent mobile belts in Kyrgyzstan and Kazakhstan. Tectonophysics, 426, 335-360.

Vandoorne, W., De Grave, J., Glorie, S., Van den haute, P., 2011. The tectonic evolution of the Chuya-Kurai zone (Siberian Altai mountains) by means of multi-method chronology. Geologica Belgica, 14, 289-292.

Vassallo, R., Jolivet, M., Ritz, J.-F., Braucher, R., Larroque, C., Sue, C., Todbileg, M., Javkhlanbold, D. (2007). Uplift age and rates of the Gurvan Bogd system (Gobi-Altay) by apatite fission track analysis. Earth and Planetary Science Letters, 259, 333-346.

Vermeesch, P., 2009. RadialPlotter: A Java application for fission track, luminescence and other radial plots. Radiation Measurements, 44, 409-410.

Vincent, S. J., Allen, M. B. (2001). Sedimentary record of Mesozoic intracontinental deformation in the eastern Junggar Basin, north-west China: response to orogeny at the Asian margin, in: Hendrix, M.S.,Davis, G.A. (Eds.), Palaeozoic and Mesozoic Tectonic Evolution of Central and Eastern Asia: from Continental Assembly to Intracontinental Deformation, Geological Society of America Memoir, pp. 341-360.

Wagner, G. A., Van den haute, P. (1992). Fission Track-Dating. Kluwer Academic Publishers, Dordrecht, 285 pp.

Wang, S., He, L., Wang, J. (2001). Thermal regime and petroleum systems in Junggar basin, northwest China. Physics of the Earth and Planetary Interiors, 126, 237-248.

Wang, B., Chen, Y., Zhan, S., Shu, L., Faure, M., Cluzel, D., Charvet, J., Laurent-Charvet, S. (2007). Primary Carboniferous and Permian paleomagnetic results from the Yili block (NW China) and their implications on the geodynamic evolution of Chinese Tianshan belt. Earth and Planetary Science Letters, 263, 288-308.

Wang, B., Cluzel, D., Shu, L., Faure, M., Charvet, J., Chen, Y., Meffre, S., de Jong, K. (2009a). Evolution of calc-alkaline to alkaline magmatism through Carboniferous convergence to Permian transcurrent tectonics, western Chinese Tianshan. International Journal of Earth Sciences, 98, 1275-1298.

Wang, Q., Li, S., Du, Z. (2009b). Differential uplift of the Chinese Tianshan since the Cretaceous: constraints from sedimentary petrography and apatite fission-track dating. International Journal of Earth Sciences, 98, 1341-1363.

Wang, S.-L., Chen, Y., Charreau, J., Wei, D.-T., Jia, D. (2013). Tectono-stratigraphic history of the southern Junggar basin: seismic profiling evidences. Terra Nova, 25, 490-495.

Wei, S. N., Cheng, J. F., Yu, D.B., Zhu, Y. F. (2011). Petrology and SHRIMP zircon ages of intrusive body III in Baogutu area, Xinjiang. Earth Science Frontiers, 18, 212-222 (in Chinese with English abstract).

Wilhem, C., Windley, B. F., Stampfli, G. M. (2012). The Altaids of Central Asia: A tectonic and evolutionary innovative review. Earth-Science Reviews, 113, 303-341.

Windley, B.F., Alexeiev, D., Xiao, W., Kröner, A., Badarch, G. (2007). Tectonic models for the accretion of the Central Asion Orogenic Belt. Journal of the Geological Society of London, 164, 31-47.

Xiao, W., Han, C., Yuan, C., Sun, M., Lin, S., Chen, H., Li, Z., Li, J., Sun, S. (2008). Middle Cambrian to Permian subduction-related accretionary orogenesis of Northern Xinjiang, NW China: Implications for the tectonic evolution of central Asia. Journal of Asian Earth Sciences, 32, 102 – 117.

Xiao, W., Huang, B., Han, C., Sun, S., Li, J. (2010). A review of the western part of the Altaids: A key to understanding the architecture of accretionary orogens. Gondwana Research, 18, 253-273.

Xiao, W., Windley, F., Allen, B., Han, C. (2013). Paleozoic multiple accretionary and collisional tectonics of the Chinese Tianshan orogenic collage. Gondwana Research, 23, 1316-1341.

Yang, W., Jolivet, M., Dupont-Nivet, G., Guo, Z., Zhang, Z., Wu, C. (2013). Source to sink relations between theTian Shan and Junggar Basin (northwest China) from Late Palaeozoic to Quaternary: evidence from detrital U-Pb zircon geochronology. Basin Research, 25, 219-240.

Yang, W., Jolivet, M., Dupont-Nivet, G., Guo, Z. (2014a). Mesozoic-Cenozoic tectonic evolution of southwestern Tian Shan: Evidence from detrital zircon U/Pb and apatite fission track ages of the Ulugqat area, Northwest China. Gondwana Research, 26, 986-1008.

Yang, G., Li, Y., Safonova, I., Yi, S., Tong, L., Seltmann, R. (2014b). Early Carboniferous volcanic rocks of West Junggar in the western Central Asian Orogenic Belt: implications for a supra-subduction system. International Geology Review, 56, 823-844.

Yang, Y.-T., Song, C.-C., He, S. (2015). Jurassic tectonostratigraphic evolution of the Junggar Basin, NW China: A record of Mesozoic intraplate deformation in Central Asia. Tectonics, 34, 86-115.

Yin, J., Yuan, C., Sun, M., Long, X., Zhao, G., Wong, K. P., Geng, H., Cai, K. (2010). Late Carboniferous high-Mg dioritic dikes in Western Junggar, NW China: Geochemical features, petrogenesis and tectonic implications. Gondwana Research, 17, 145-152.

Yin, J., Long, X., Yuan, C., Sun, M., Zhao, G., Geng, H. (2013). A Late Carboniferous - Early Permian slab window in the West Junggar of NW China: Geochronological and geochemical evidence from mafic to intermediate dikes. Lithos, 175-176, 146-162.

Yu, S., Chen, W., Evans, N. J., McInnes, B. I. A., Yin, J., Sun, J., Li, J., Zhang, B. (2014). Cenozoic uplift, exhumation and deformation in het north Kuqa Depression, China as constrained by (U-Th)/He thermochronometry. Tectonophysics, 630, 166-182.

Yuan, W.-M., Carter, A., Dong, J.-Q., Bao, Z., An, Y., Guo, Z. (2006). Mesozoic-Tertiary exhumation history of the Altai Mountains, northern Xinjiang, China: new constraints from apatite fission track data. Tectonophysics, 412, 183-193.

Zhang, Z.H., Mao, J.W., Du, A.D., Pirajno, F., Wang, Z.L., Chai, F.M., Zhang, Z.C., Yang, J.M. (2008). Re-Os dating of two Cu-Ni sulfide deposits in northern Xinjiang, NW China and its geological significance. Journal of Asian Earth Sciences, 32, 204 - 217.

Zhao, L., He, G. (2013). Tectonic entities connection between West Junggar (NW China) and East Kazakhstan. Journal of Asian Earth Sciences, 72, 25-32.

Zhou, T., Yuan, F., Fan, Y., Zhang, D., Cooke, D., Zhao, G. (2008). Granites in the Sawuer region of the west Junggar, Xinjiang Province, China: Geochronological and geochemical characteristics and their geodynamic significance. Lithos, 106, 191-206.

Zhu, Y.F., He, G.Q., An, F. (2007). Geological evolution and metallogeny in the core part of the Central Asian metallogenic domain. Geological Bulletin of China, 26, 1167 - 1177.

Zorin, Y. A. 1999. Geodynamics of the western part of the Mongolia-Okhotsk collisional belt, Trans-Baikal region (Russia) and Mongolia. Tectonophysics, 306, 33-56.

Tables and captions

Table 1: Sample localities, lithology and used methods. AFT = Apatite Fission-Track dating, ZUPb = zircon U-Pb dating.

Sample	Latitude (N)	Longitude (E)	Alt. (m)	Sample site	Lithology	Method
11-01	45°16'25.5"	079°20'49.0"	1000	Kazakh West Junggar Range	granite	AFT, ZUPb
11-07	44°53'39.3"	079°01'56.9"	1718	Kazakh West Junggar Range	diorite	AFT, ZUPb
11-09	44°53'36.1"	079°09'38.1"	1763	Kazakh West Junggar Range	diorite	AFT, ZUPb
11-11	44°53'05.9"	078°58'42.1"	2029	Kazakh West Junggar Range	diorite	AFT
11-20	44°53'05.9"	078°58'42.1"	2029	Kazakh West Junggar Range	granite	AFT, ZUPb
SK-17	44°14' 35.0"	079°28'16.3"	1168	Altyn-Emel Range	tuff	ZUPb
SK-21	44°11'07.4"	078°32'25.3"	1542	Altyn-Emel Range	granodiorite	AFT, ZUPb
SK-22	44°28'44.1"	077°55'38.8"	930	Malaysari Range	tuff	ZUPb
11-27	43°03'21.5"	076°58'59.2"	2510	Trans-Ili Range	diorite	AFT
11-28	43°02'22.3"	076°56'40.0"	3379	Trans-Ili Range	granite	AFT
SK-31	42°54'54.0"	076°13'05.2"	3076	Trans-Ili Range	gneiss	AFT
SK-32	42°55'10.2"	076°13'00.7"	3357	Trans-Ili Range	gneiss	AFT
SK-05A	43°20'24.0"	078°56'01.6"	1337	Sogeti Range	granite	AFT, ZUPb
10-20	43°19'38.1"	074°51'57.0"	904	Zhetyzol Range	granite	AFT
10-40	45°42'31.5"	073°30'20.4"	344	Near Priozersk (W of Lake Balkhash)	granite	AFT
10-42	47°21'39.3"	074°44'18.2"	576	Bektauta mountain (N of Lake Balkhash)	granite	AFT

Table 2: Operating conditions for ZUPb LA-ICP-MS analysis at the laboratory of Géosciences Rennes, Université Rennes 1, France.

Laser-ablation system ESI NWR193UC	
Laser type/wavelength	Excimer 193 nm
Pulse duration	< 5 ns
Energy density on target	~ 7 J/cm^2
ThO^+/Th^+	< 0.5%
He gas flow	800 ml/min
N_2 gas flow	4 ml/min
Laser repetition rate	3 Hz
Laser spot size	25 µm
ICP-MS Agilent 7700x	
RF power	1350 W
Sampling depth	5.0-5.5 mm (optimized daily)
Carrier gas flow (Ar)	~ 0.85 l/min (optimized daily)
Coolant gas flow	16 l/min
Data acquisition protocol	Time-resolved analysis
Scanning mode	Peak hopping, one point per peak
Detector mode	Pulse counting, dead time correction applied, and analog mode when signal intensity > ~ 10^6 cps
Isotopes determined	^{204}(Hg + Pb), ^{206}Pb, ^{207}Pb, ^{208}Pb, ^{232}Th, ^{238}U
Dwell time per isotope	10-30 ms
Sampler, skimmer cones	Ni
Extraction lenses	X type

Table 3: Zircon U-Pb LA–ICP–MS dating results. Each parameter in the table is calculated based on the arithmetic mean. Multiple age-components within one sample (as interpreted from the Tera-Wasserburg diagrams in Fig. 5) are listed separately. [a] = U and Pb concentrations and Th/U ratios calculated relative to the GJ-1 zircon standard. [b] = Number of analyses used to calculate the preferred zircon U/Pb age. [c] = Preferred ages calculated with Isoplot (Ludwig, 2003) after interpretation based on the Tera-Wasserburg diagrams in Fig. 5. A more detailed table, listing the results for each analyzed spot, can be found in Supplementary Table S1.

Sample Name	Sample site	Lithology	U[a] (ppm)	Pb[a] (ppm)	Th/U[a]	N[b]	Preferred age[c] (Ma)	Age calculation (weighted mean)
11-01	Kazakh W Junggar R.	granite	385	17	0.34	18	298 ± 4	$^{206}Pb/^{238}U$ age
11-07	Kazakh W Junggar R.	granodiorite	588	26	0.73	29	297 ± 2	$^{206}Pb/^{238}U$ age
11-09	Kazakh W Junggar R.	granodiorite	4876	188	0.41	17	260 ± 3	$^{206}Pb/^{238}U$ age
11-20	Kazakh W Junggar R.	granite	799	45	0.68	15	296 ± 2	$^{206}Pb/^{238}U$ age
SK-17	Altyn-Emel Range	tuff	214	8	0.60	16	331 ± 2	$^{206}Pb/^{238}U$ age
			226	8	3.89	7	311 ± 4	$^{206}Pb/^{238}U$ age
SK-21	Altyn-Emel Range	granodiorite	137	9	0.75	34	341 ± 2	$^{206}Pb/^{238}U$ age
SK-22	Malaysari Range	tuff	167	12	1.53	16	320 ± 2	$^{206}Pb/^{238}U$ age
SK-05A	Sogeti Range	granite	241	15	0.73	8	351 ± 3	$^{206}Pb/^{238}U$ age
			227	13	0.70	17	332 ± 2	$^{206}Pb/^{238}U$ age

Table 4: Apatite Fission Track analyses results. n is the number of counted grains. ρ_s and ρ_i correspond to the density of spontaneous tracks (in the apatite) and induced tracks (in the external detector, ED) respectively. ρ_d-values are interpolated values of the density of induced tracks in the ED irradiated against regularly spaced glass dosimeters (IRMM-540). ρ_s and ρ_i are expressed as 10^6 tracks/cm^2; ρ_d is expressed as 10^5 tracks/cm^2. N_s and N_i are the number of counted spontaneous tracks (in the apatite) and induced tracks (in the ED) respectively. N_d is the interpolated value of the number of counted induced tracks in the ED irradiated against regularly spaced glass dosimeters. P(χ^2) is the chi-squared probability that the dated grains have a constant ρ_s/ρ_i-ratio. For the calculation of the AFT zeta-age t(ζ) (in Ma), a ζ-value of 229.8 ± 4.9 a.cm^2 was used, based on Durango and Fish Canyon Tuff age standards. AFT ages were also calculated as central ages t(c) (in Ma). AFT length results are reported as mean track length (l_m in µm) with standard deviation σ (in µm), obtained from the measurement of an amount (n_l) of natural, horizontal confined tracks. Measurements of D_{par} are in µm. For some samples, no AFT length data is reported due to low spontaneous track densities and/or a low number of suitable grains. Length data of sample SK-31 (in italic) is considered as a very low amount, and thermal history modeling based on this data should be treated with caution.

Sample	n	ρ_s (± 1σ)	N_s	ρ_i (± 1σ)	N_i	ρ_d (± 1σ)	N_d	ρ_s/ρ_i (± 1σ)	$P(\chi^2)$	t (ζ) ± 1σ (Ma)	t (c) ± 1σ (Ma)	n_l	l_m (± 1σ) (μm)	D_{par} (± 1σ) (μm)
Kazakh West Junggar & Altyn-Emel Ranges														
11-01	54	3.710 (0.105)	1240	1.576 (0.067)	562	3.227 (0.071)	2065	2.344 (0.119)	0.98	86.3 ± 5.1	81 ± 4	58	11.8 (1.8)	1.6 (0.2)
11-07	6	0.432 (0.078)	31	0.277 (0.062)	20	3.244 (0.071)	2076	1.544 (0.443)	0.95	57.3 ± 16.5	58 ± 16	–	–	–
11-09	28	0.775 (0.021)	1332	0.397 (0.015)	685	3.298 (0.072)	2110	2.031 (0.095)	0.77	76.5 ± 4.3	73 ± 3	100	14.1 (1.2)	3.0 (0.3)
11-11	56	0.637 (0.021)	918	0.347 (0.158)	483	3.309 (0.072)	2118	2.055 (0.116)	1.00	77.7 ± 5.0	72 ± 4	72	14.0 (1.1)	2.5 (0.3)
11-20	11	0.723 (0.042)	295	0.278 (0.026)	111	3.333 (0.072)	2133	2.579 (0.287)	0.95	98.0 ± 11.3	101 ± 11	–	–	–
SK-21	34	1.174 (0.036)	1064	0.455 (0.022)	414	3.105 (0.070)	1987	2.781 (0.161)	0.76	98.5 ± 6.5	91 ± 6	104	13.7 (1.2)	2.4 (0.4)
Trans-Ili, Sogeti & Zhetyzol Ranges														
10-20	17	3.692 (0.096)	1498	1.269 (0.057)	500	3.187 (0.071)	2039	3.023 (0.157)	0.48	109.8 ± 6.6	108 ± 6	103	13.5 (1.1)	2.0 (0.3)
11-27	58	0.150 (0.007)	414	0.583 (0.014)	1709	3.345 (0.072)	2141	0.264 (0.014)	0.78	10.1 ± 0.6	9 ± 1	–	–	–
11-28	58	0.330 (0.011)	926	0.772 (0.016)	2265	3.356 (0.072)	2148	0.435 (0.017)	0.82	16.8 ± 0.8	16 ± 1	65	13.9 (1.5)	2.0 (0.2)
SK-05A	45	0.393 (0.017)	529	0.117 (0.009)	154	3.087 (0.070)	1976	3.653 (0.335)	0.99	128.3 ± 12.4	121 ± 11	–	–	–
SK-31	50	0.423 (0.011)	1410	0.189 (0.007)	645	3.120 (0.070)	1997	2.388 (0.114)	0.88	85.1 ± 4.8	78 ± 4	*27*	*13.2 (1.5)*	*2.1 (0.3)*
SK-32	41	0.504 (0.014)	1309	0.168 (0.008)	415	3.127 (0.070)	2002	3.383 (0.191)	1.00	120.4 ± 7.7	112 ± 6	40	13.8 (1.2)	1.7 (0.2)
NW Lake Balkhash														
10-40	19	0.354 (0.022)	259	0.162 (0.016)	107	3.196 (0.071)	2045	2.469 (0.284)	0.97	90.0 ± 10.7	88 ± 10	–	–	–
10-42	6	1.625 (0.126)	167	0.803 (0.092)	77	3.216 (0.071)	2058	2.013 (0.277)	0.87	74.0 ± 10.4	80 ± 11	–	–	–

Figures and captions

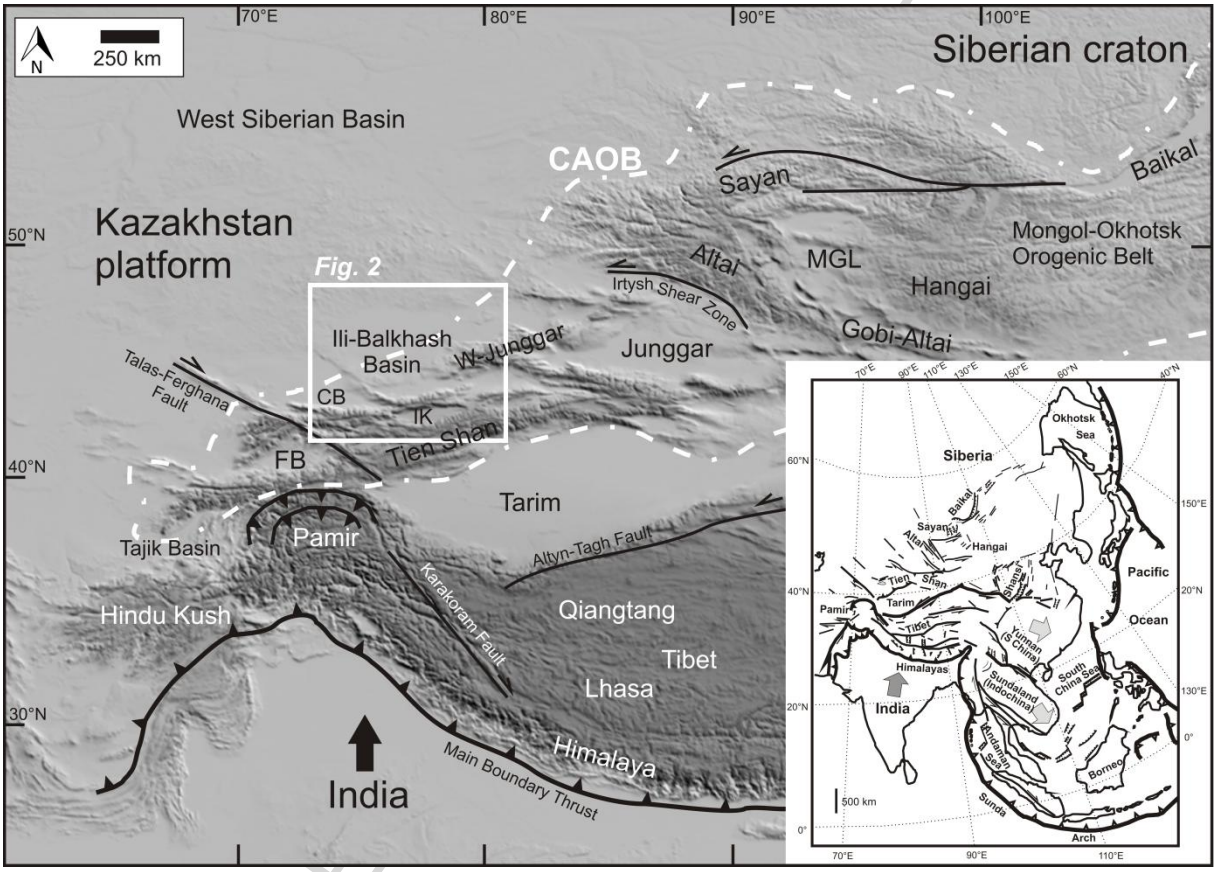

Fig. 1. General topographic and tectonic map of Central Asia with indication of the Central Asian Orogenic Belt (CAOB) and the Ili-Balkhash study area (white square detailed in Figure 2). CB = Chu Basin, FB = Ferghana Basin, IK = Issyk-Kul Basin, MGL = Mongolian Great Lakes, W-Junggar = West Junggar Mountains.

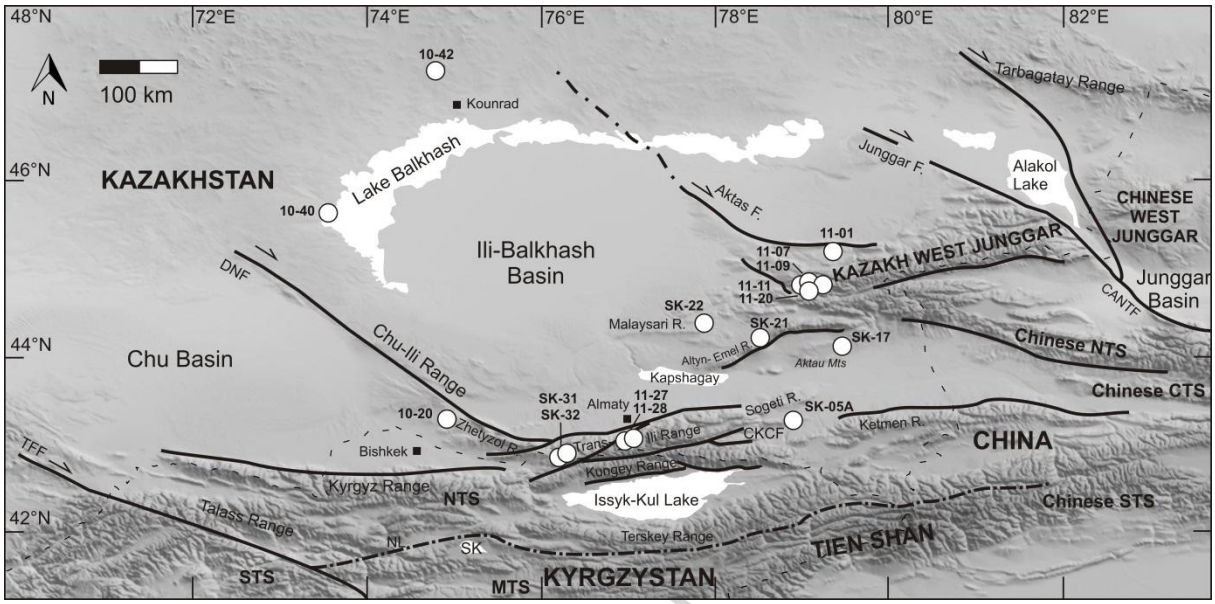

Fig. 2. Topographic map of the Ili-Balkhash study area. Sample sites are displayed as white dots. Main faults after Campbell et al. (2013), Choulet et al. (2011) and Delvaux et al. (2001). CANTF = Chingiz – Alakol – North Tien Shan Fault, CKCF = Chon – Kemin – Chilik Fault, DNF = Dzhalair – Naiman Fault, NL = Nikolaev Line, TFF = Talas – Ferghana Fault. CTS = Central Tien Shan, MTS = Middle Tien Shan, NTS = North Tien Shan, STS = South Tien Shan. F. = Fault, Mts = Mountains, R. = Range, SK = Song Kul lake.

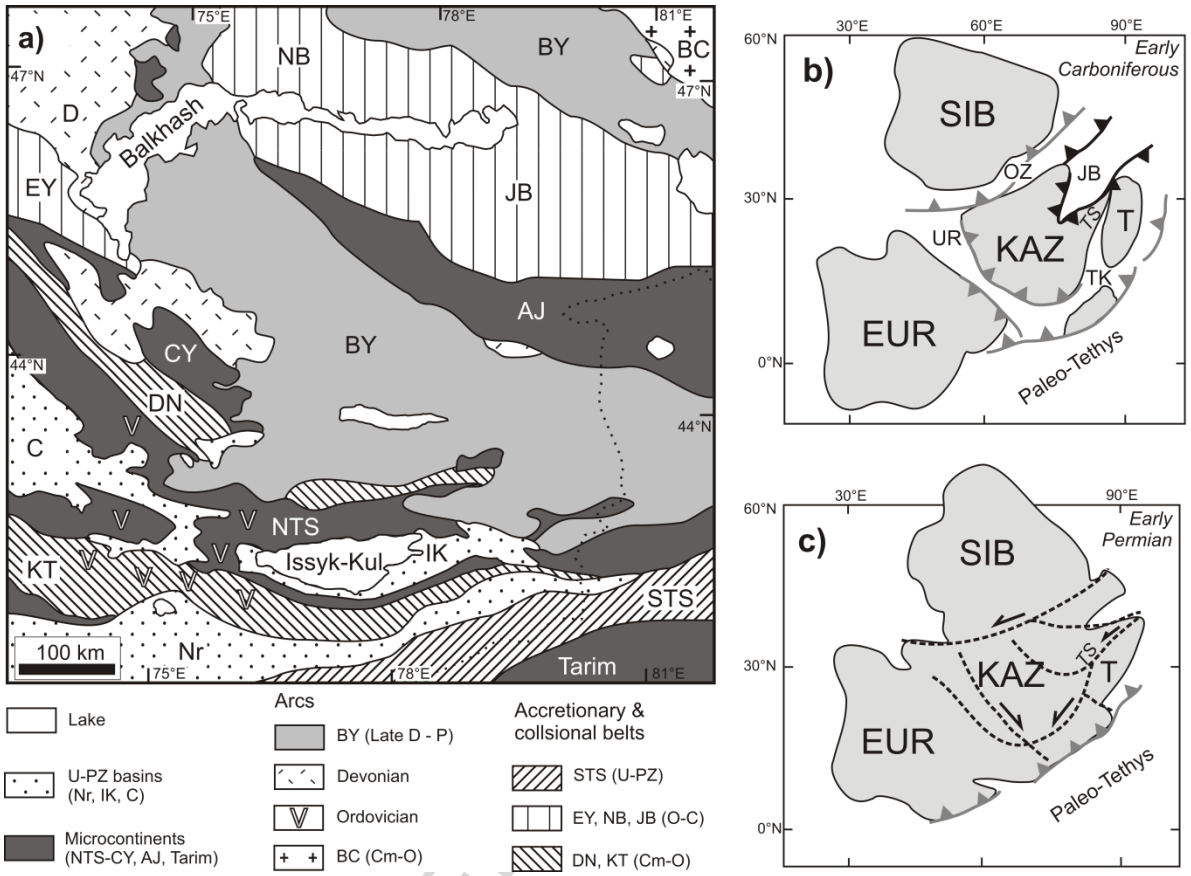

Fig. 3. (a) Schematic overview of the key basement units of SE Kazakhstan based on Alexeiev et al. (2011), Kröner et al. (2013) and Windley et al. (2007) and references therein. AJ = Aktau-Junggar, BC = Boshchekul-Chingiz, BY = Balkhash-Ili, C = Chu, CY = Chu-Ili, DN = Dzhailair-Naiman, EY = Erementau-Ili, IK = Issyk-Kul, JB = Junggar-Balkhash, KT = Kyrgyz-Terskey, NB = North Balkhash, Nr = Naryn, NTS = North Tien Shan, STS = South Tien Shan. U = Upper, PZ = Paleozoic, Cm = Cambrian, O = Ordovician, D = Devonian, C = Carboniferous, P = Permian. (b-c) Schematic reconstruction of the geodynamic setting of Siberia (SIB), Kazakhstan (KAZ), Europa (EUR) and Tarim (T) during the early Carboniferous (b) and early Permian (c) based on Abrajevitch et al. (2008), Filippova et al. (2001) and Windley et al. (2007). Emphasis on main sutures and faults (dashed lines) and subduction zones (solid lines): Junggar-Balkhash subduction zone in black; Siberian, Turkestan and Paleo-Tethyan subduction zones in grey. JB = Junggar-Balkhash Ocean, OZ = Ob-Zaisan Ocean, TK = Turkestan Ocean, UR = Uralian Ocean, TS = Tien Shan.

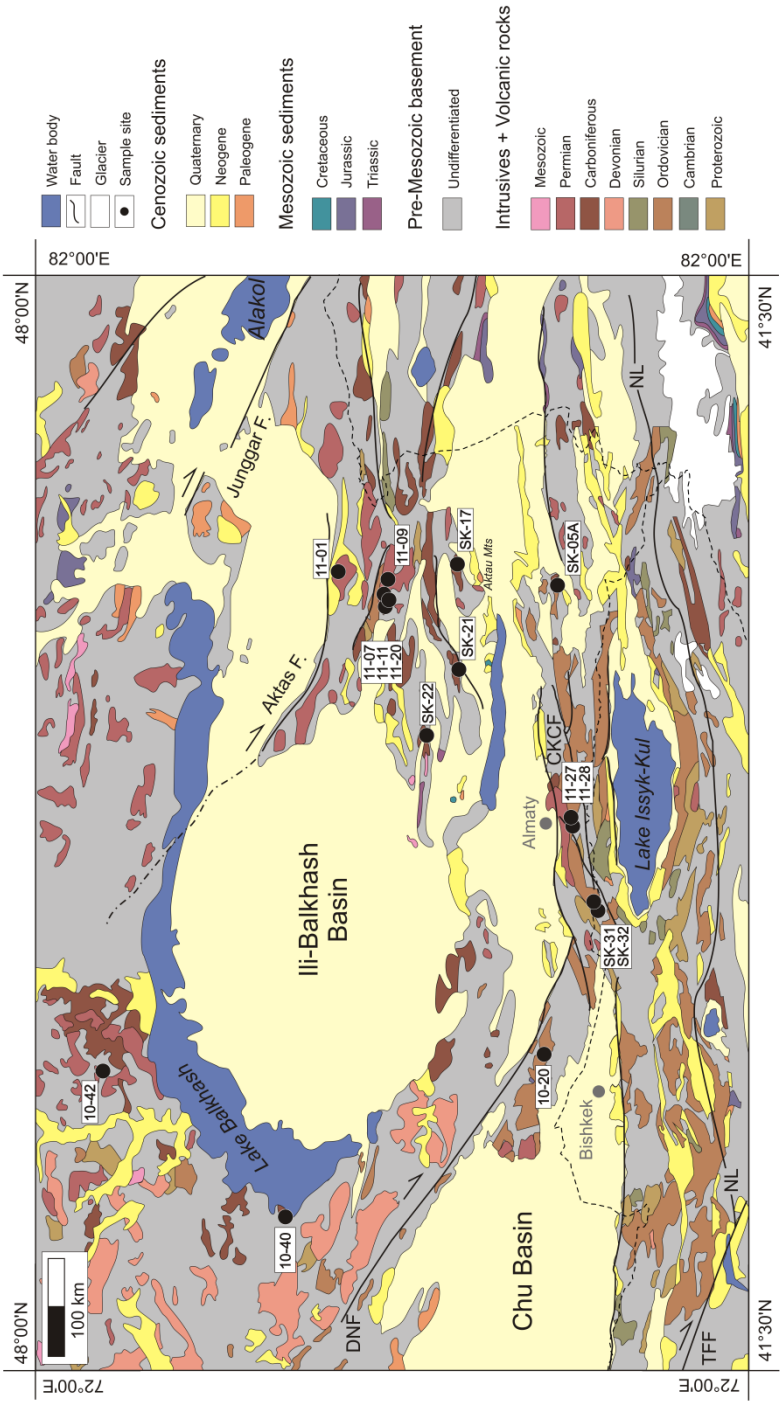

Fig. 4. Simplified geological map of the Ili-Balkhash study area based on the geological map of Western China and adjacent regions (IGCAGS, 2006) and other more detailed maps. Sample sites are displayed as black dots. Main faults after Campbell et al. (2013), Choulet et al. (2011) and Delvaux et al. (2001). CKCF = Chon – Kemin – Chilik Fault, DNF = Dzhalair – Naiman Fault, NL = Nikolaev Line, TFF = Talas – Ferghana Fault. F. = Fault, Mts = Mountains.

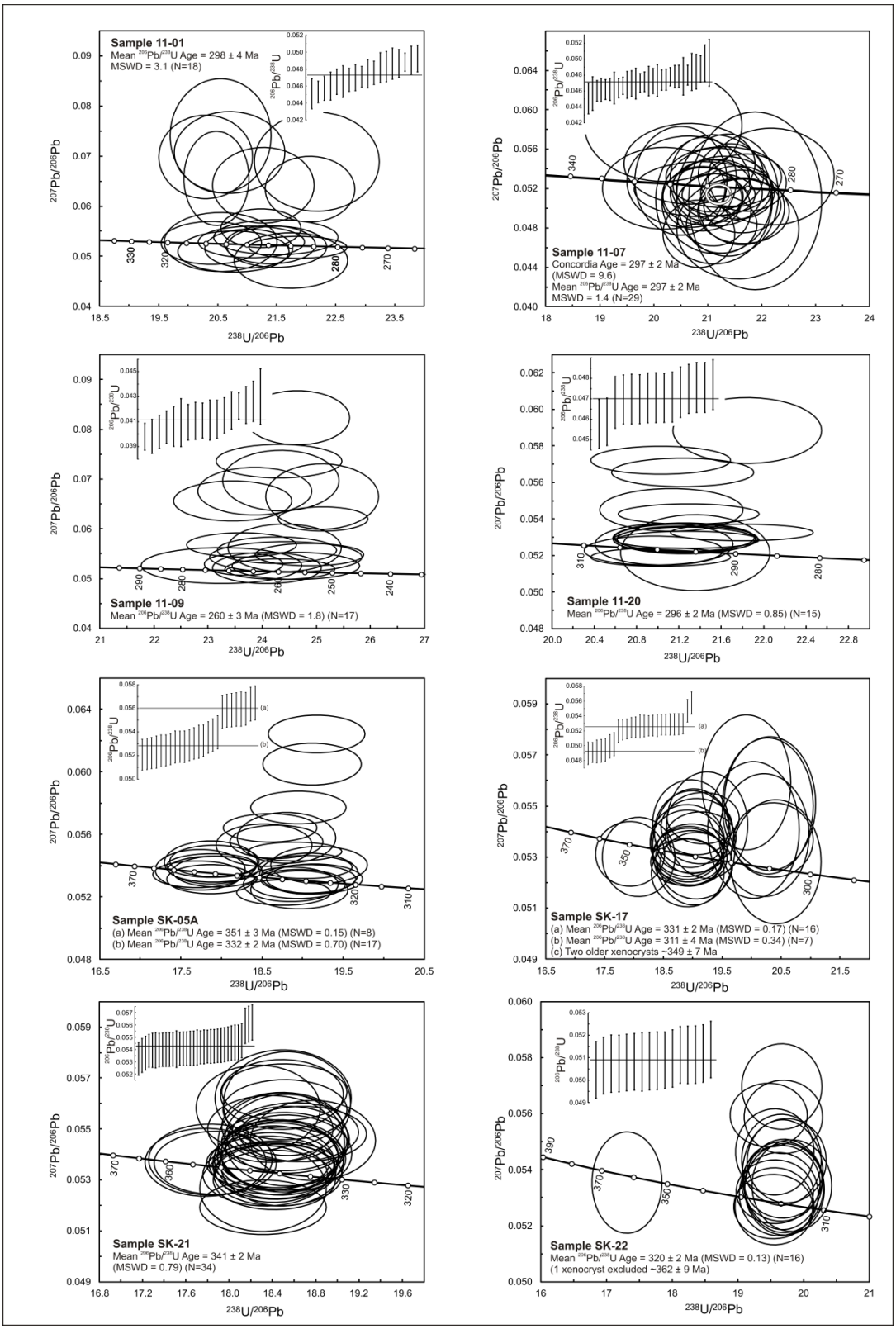

Fig. 5. Zircon U-Pb Tera-Wasserburg diagrams with insets of weighted mean $^{206}Pb/^{238}U$ ratios for each analyzed sample (drawn with Isoplot; Ludwig, 2003). All data-point error ellipses are calculated at 2σ level.

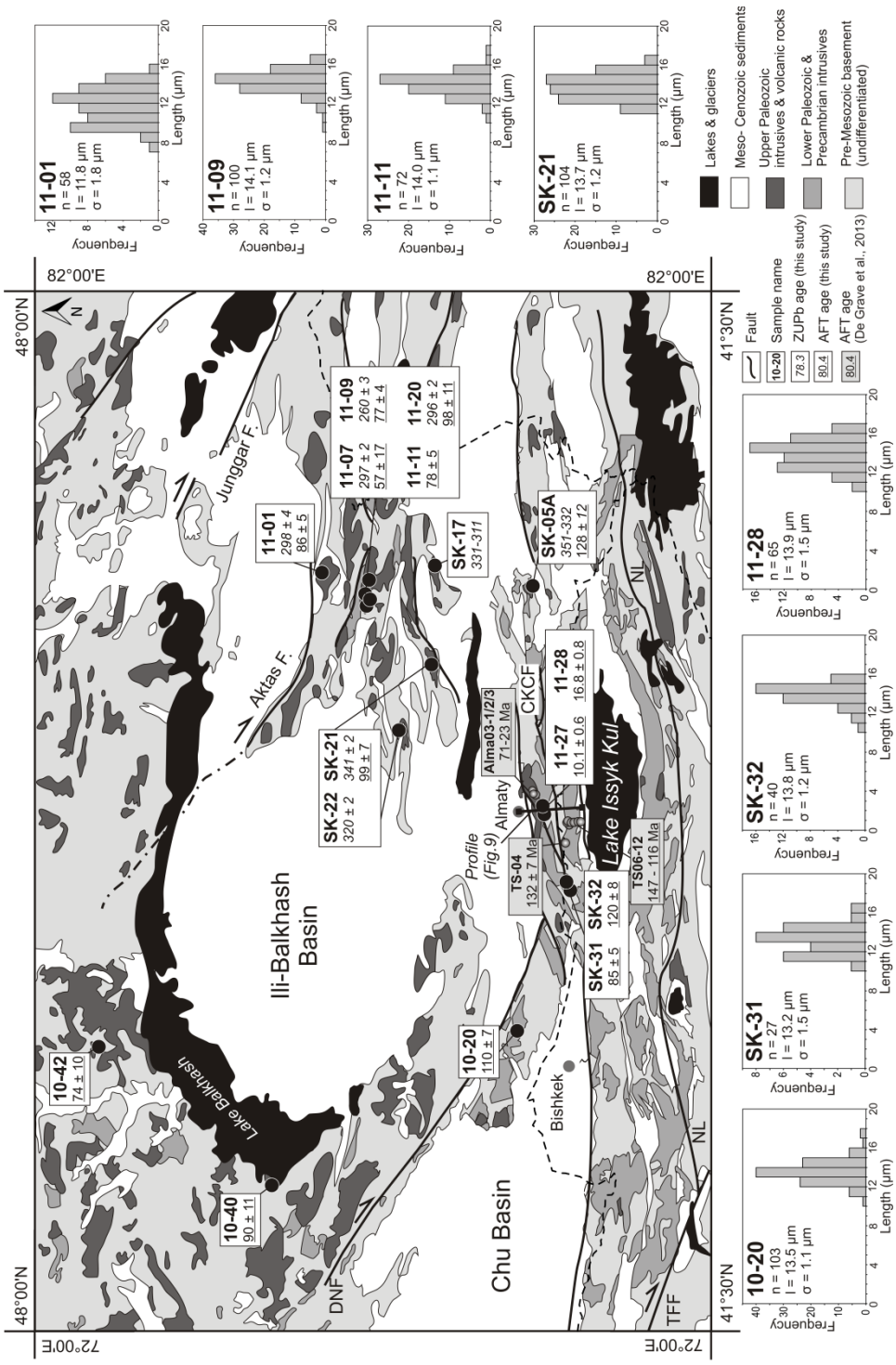

Fig. 6. Schematic geological map of the Ili-Balkhash study area with indication of sample sites (black dots), ZUPb- and AFT-ages (in Ma, white squares), and AFT length-frequency histograms. Main faults after Campbell et al. (2013), Choulet et al. (2011) and Delvaux et al. (2001). CKCF = Chon – Kemin – Chilik Fault zone, DNF = Dzhalair – Naiman Fault, NL = Nikolaev Line, TFF = Talas – Ferghana Fault.

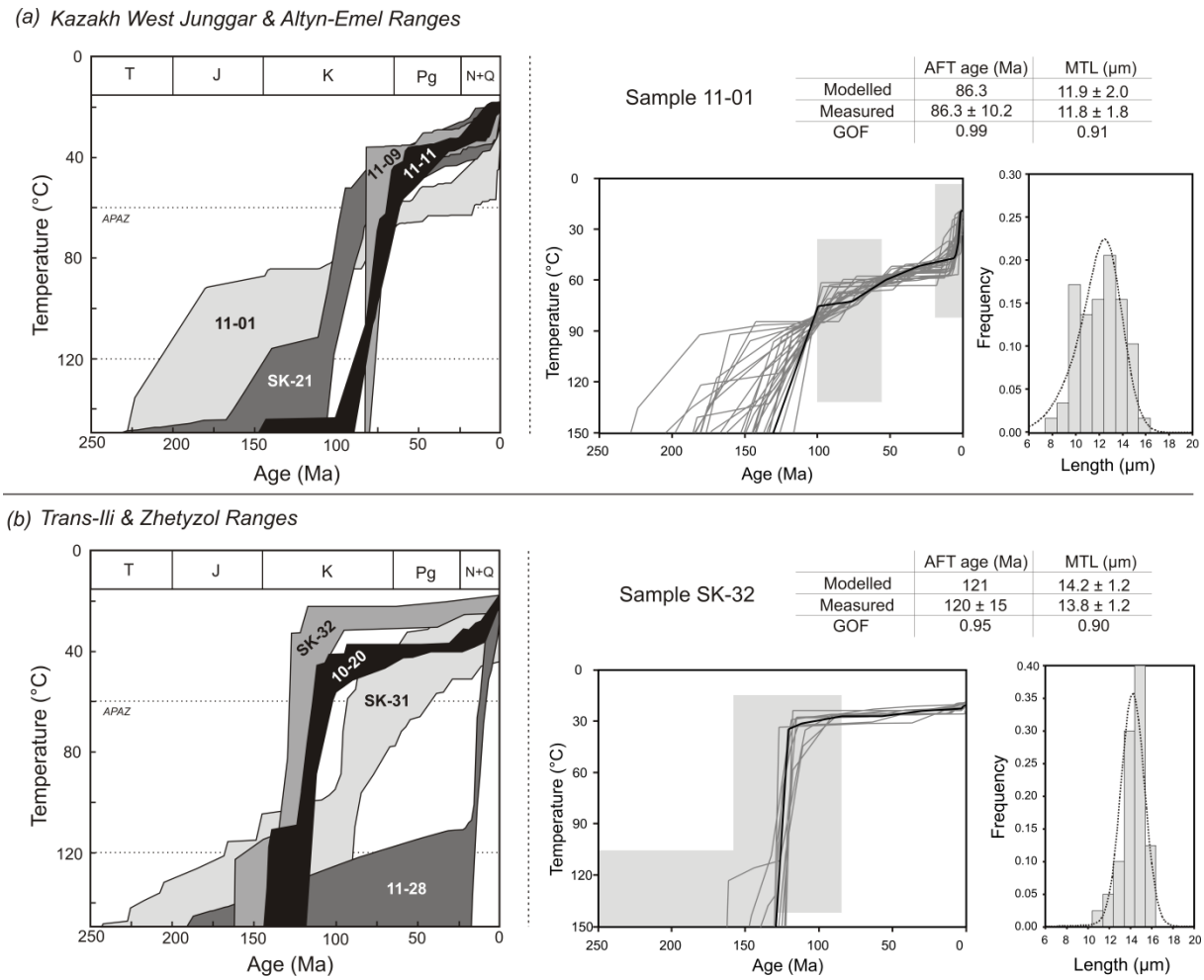

Fig 7. Thermal history model results produced by HeFTy (Ketcham, 2005) for eight samples from (a) the Kazakh West Junggar and Altyn-Emel Ranges and (b) the Trans-Ili and Zhetyzol Ranges. On the left: overview of the models shown as cooling path envelopes based on "good" fits. On the right: individual model results for a representative example. Shown cooling paths in grey correspond to "good" fits (acceptable fits are not shown). Time-temperature constraints are indicated as grey boxes. Track length distributions are shown as histograms. Black line corresponds to the best fit. APAZ = Apatite Partial Annealing Zone; MTL = mean track length; GOF = goodness of fit. Calculated parameters based on 2SE uncertainties. Models for the other six samples can be found in the Supplementary Figure S2.

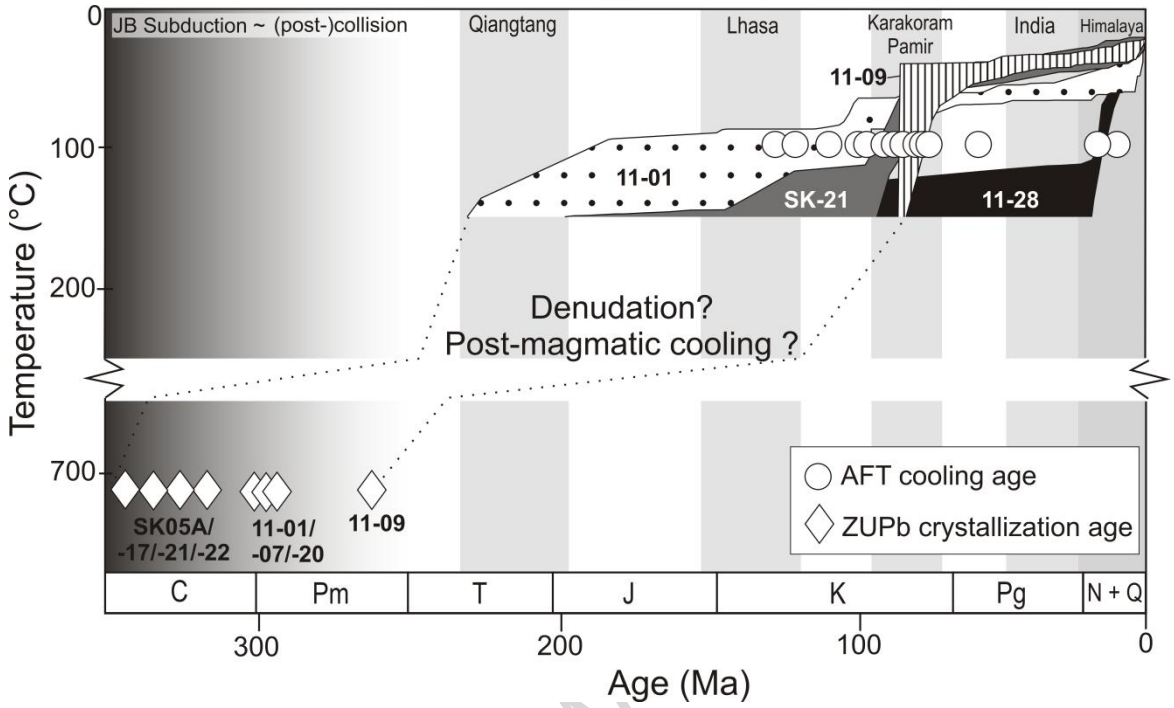

Fig. 8: Overview of the obtained ages by ZUPb and AFT dating and some representative thermal history models for the sampled basement ranges in SE Kazakhstan. The ZUPb crystallization ages can be related to a transition period from subduction of the Junggar-Balkhash (JB) Ocean to collisional and post-collisional magmatism. The supposed driving forces for the late Mesozoic and Cenozoic exhumation of the basement are believed to be related to far-field accretion-collisions events, which are schematically shown as grey vertical bars: the Mesozoic Cimmerian collisions (Qiangtang, Lhasa, Karakoram-Pamir) and Cenozoic India-Eurasia collision.

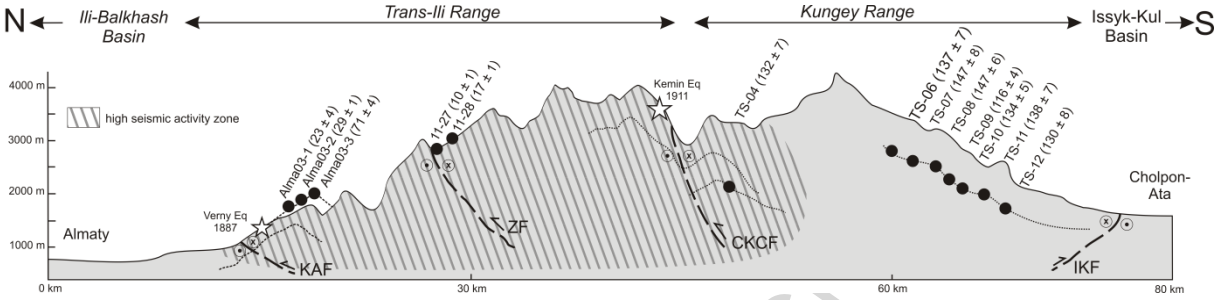

Fig. 9: Topographic cross-section from Almaty (SE Kazakhstan) to Cholpon-Ata (NE Kyrgyzstan) with indication of sample sites (black dots). Position of cross-section as in Fig. 6. Shown samples with AFT ages (in Ma) are partly from this study (11-27, 11-28) and partly from De Grave et al. (2013) (ALMA03-01/02/03, TS-04, TS-06/07/08/09/10/11/12). Indicated faults are based on Buslov et al. (2003a), Delvaux et al. (2001), Torizin et al. (2009): CKCF = Chon-Kemin-Chilik Fault, IKF = Issyk-Kul Fault, KAF = Karakunug-Almaty Fault, ZF = Zailisky or Trans-Ili Fault. Surface rupture locations for the Verny (1887) and Kemin (1911) earthquakes (eq) are after Abdrakhmatov et al. (2002). The outline of the high seismic activity zone is based on Torizin et al. (2009).

Highlights

- Carboniferous-Permian zircon U-Pb crystallization ages are found in SE-Kazakhstan.
- AFT dating of SE-Kazakhstan basement samples mainly reveals Cretaceous ages.
- Thermal history models indicate distinct late Mesozoic basement cooling.
- Two Miocene AFT ages along inherited faults demonstrate late Cenozoic reactivation.